Complex Förster Energy Transfer Interactions between Semiconductor Quantum Dots and a Redox-Active Osmium Assembly

Michael H. Stewart,[†,△,*] Alan L. Huston,[†,△] Amy M. Scott,[‡] Alexander L. Efros,[§] Joseph S. Melinger,[⊥] Kelly Boeneman Gemmill,[∥] Scott A. Trammell,[∥] Juan B. Blanco-Canosa,[#] Philip E. Dawson,[#] and Igor L. Medintz[∥,*]

[†]Optical Sciences Division, Code 5611, [§]Center for Computational Materials Science, Code 6393, [⊥]Electronic Science and Technology, Code 6812, and [∥]Center for Bio/Molecular Science and Engineering, Code 6900, U.S. Naval Research Laboratory, Washington, D.C. 20375, United States, [‡]Department of Chemistry, Columbia University, New York, New York 10027, United States, and [#]Departments of Cell Biology and Chemistry, The Scripps Research Institute, La Jolla, California 92037, United States. [△]Contributed equally.

ABSTRACT The ability of luminescent semiconductor quantum dots (QDs) to engage in diverse energy transfer processes with organic dyes, light-harvesting proteins, metal complexes, and redox-active labels continues to stimulate interest in developing them for biosensing and light-harvesting applications. Within biosensing configurations, changes in the rate of energy transfer between the QD and the proximal donor, or acceptor, based upon some external (biological) event form the principle basis for signal transduction. However, designing QD sensors to function optimally is predicated on a full understanding of all relevant energy transfer mechanisms. In this report, we examine energy transfer between a range of CdSe–ZnS core–shell QDs and a redox-active osmium(II) polypyridyl complex. To facilitate this, the Os complex was synthesized as a reactive isothiocyanate and used to label a hexahistidine-terminated peptide. The Os-labeled peptide was ratiometrically self-assembled to the QDs *via* metal affinity coordination, bringing the Os complex into close proximity of the nanocrystal surface. QDs displaying different emission maxima were assembled with increasing ratios of Os–peptide complex and subjected to detailed steady-state, ultrafast transient absorption, and luminescence lifetime decay analyses. Although the possibility exists for charge transfer quenching interactions, we find that the QD donors engage in relatively efficient Förster resonance energy transfer with the Os complex acceptor despite relatively low overall spectral overlap. These results are in contrast to other similar QD donor–redox-active acceptor systems with similar separation distances, but displaying far higher spectral overlap, where charge transfer processes were reported to be the dominant QD quenching mechanism.

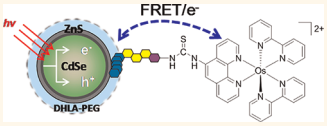

KEYWORDS: semiconductor · quantum dot · peptide · osmium · redox · electron transfer · peptide · metal complex · polypyridyl · FRET · charge transfer · metal affinity · coordination

The unique electronic and photophysical properties of luminescent semiconductor nanocrystals or quantum dots (QDs) allow them to engage in different types of resonance energy or electron transfer with diverse materials ranging from fluorescent proteins to fullerenes.[1−6] These properties have stimulated a growing interest in harnessing the underlying intrinsic processes for charge separation and energy-harvesting applications along with applying them in different biosensing formats.[1−3,5,7,8] For the latter, the QDs fulfill several roles including acting as a central nanoscale platform for displaying multiple biorecognition molecules along with functioning as intrinsic donors or acceptors that undergo fluorescence modulation in response to the presence of target analyte.[1−3,5,7] In terms of demonstrated transfer processes, hydrophilic QDs have been shown to be excellent donors for Förster resonance energy transfer (FRET) with diverse acceptor materials including organic dyes, polymers, and fluorescent proteins.[1,2,5,9] Several reports have also shown them to be equally adept in the role of FRET acceptor especially for terbium and other long-lifetime metal-chelate fluorescent donors.[10−12] Beyond FRET, QDs have been shown to engage in dipole–dipole-type energy transfer (ET) with nonfluorescent acceptor materials such as gold nanoparticles and carbon allotropes, although the underlying processes in these configurations have not been fully elucidated.[4,13−16] QD photoluminescence (PL) intensity is also well known to be sensitive to charge transfer (CT) processes or the presence of charges on their surface and/or in their environment.[7,17,18] This sensitivity potentially allows QD PL to be coupled to changes in CT, thereby providing a fluorescent signal transduction modality for monitoring an underlying electronic process. For example, coupling the neurotransmitter dopamine to hydrophilic QDs allowed the hybrid nanocrystal–complexes to function as a charge-transfer-coupled pH sensor.[19] In this configuration, dopamine's pH-dependent

* Address correspondence to Michael.stewart@nrl.navy.mil, Igor.medintz@nrl.navy.mil.

Received for review March 16, 2012 and accepted May 23, 2012.

Published online June 07, 2012
10.1021/nn301177h

oxidation to quinone allowed it to become an increasingly potent electron acceptor that quenched QD PL in a manner directly reflecting the surrounding pH.

Recent work has suggested that small redox-active metal complexes may be particularly useful for pairing with QDs to achieve designer ET interactions.[2,3,7,20,21] These materials have several useful attributes that can contribute directly to this role including the following: (i) precursors for many of the relevant metal complexes are commercially available and not costly; (ii) the chemistry required to assemble the final complexes is relatively simple with high yields; (iii) complexes can be easily activated to a reactive form for specific labeling of (bio)molecules; (iv) the valence state and redox properties of many of these metal complexes can be tuned by altering the surrounding chelating substituents in the complex; (v) the donor–acceptor separation distance can be altered; and (vi) overall, the properties of these molecules are relatively well understood, and detailed reference literature is available describing them.[17,22–24] Although a variety of transition and other metals such as iridium, rhenium, and iron are usually prominent in these complexes, it is a tetraammine ruthenium(II) phenanothroline complex that has been extensively prototyped in QD biosensing formats. Benson's group labeled maltose binding protein, intestinal fatty acid binding protein, and a thrombin-binding DNA aptamer with a maleimido-activated Ru-phenanthroline and then attached them to QDs to assemble sensors for maltose, fatty acids, and thrombin, respectively.[21,25,26] Within these composite Ru–QD assemblies, it was postulated that analyte binding to the protein or aptamer resulted in a structural rearrangement that altered the distance between QD–Ru and the electron transfer rate, and thus the QD PL, to provide an output signal. Subsequent work using peptides labeled with the same Ru complex demonstrated that the electron transfer rate was highly dependent on the relative position of the QD and metal complex oxidation levels and directly reflected the quantity of metal brought in close proximity of the nanocrystal surface.[20] Spectroscopic analysis supported an oxidative process reflecting electron transfer from the Ru complex to the QD. Importantly, testing of identical QD assemblies where peptides were labeled with either ferrocene or Ru-bipyridine phenanthroline complexes displaying unfavorable oxidation levels did not affect QD PL. Understanding this QD–Ru ET process allowed subsequent design of a QD–Ru–peptide platform that could quantitatively monitor enzymatic proteolysis along with demonstration of a simultaneous eight-color multiplex QD CT configuration.[20,27] In related studies, Sykora elegantly showed that QDs could engage in CT with $Ru(bpy)_3$ complexes *via* a hole transfer from the QD to the Ru.[28]

The utility apparent from just this one Ru-to-QD-metal interaction suggests that assembling a library of similar CT donor/acceptor complexes would certainly benefit development of QD biosensors. This, however, is directly predicated on a full understanding of each of the underlying ET processes. Several studies have described how similar osmium(II) polypyridyl complexes can function as either quenchers in electron transfer systems or photoinduced electron donors for TiO_2 and ZrO_2 semiconductor nanoparticles.[29–33] Interest in realizing similar ET processes with CdSe/ZnS core/shell QDs led us to investigate their interactions with a weakly phosphorescent Os polypyridyl complex (Figure 1). To facilitate this, the Os complex was first activated to an amine-reactive isothiocyanate form and used to label a hexahistidine-terminated peptide. This allowed for subsequent ratiometric conjugation to the QDs *via* metal affinity coordination. QDs were assembled with increasing ratios of Os–peptide complex and subjected to detailed steady-state, ultrafast transient absorption, and lifetime decay spectroscopic analyses. The results demonstrate that the QD quenching observed in the Os conjugates was completely dominated by FRET and not CT despite very low intrinsic spectral overlap. These findings are in stark contrast to those of similar QD-donor redox-acceptor systems, manifesting much stronger underlying spectral overlap, where both FRET and high rates of CT were reported.[34–36]

RESULTS

Osmium Isothiocyanate, Peptide Labeling, and Spectral Overlap with Quantum Dots. The Os polypyridyl complex was assembled using coordination chemistry as described[37] in three steps from $(NH_4)_2[OsCl_6]$. First, $(NH_4)_2[OsCl_6]$ was treated with bipyridine to yield $[Os(bpy)_2]Cl_2$, followed by addition of 5-amino-1,10-phenanthroline (phen-NH_2) to generate $[Os(bpy)_2$-(phen-NH_2)$](PF_6)_2$, referred to as Os-bpy. Then, the amine group of phen-NH_2 was converted to a reactive isothiocyanate group (NCS) using thiophosgene, allowing the final assembled metal complex (Figure 1A) to be used for covalent conjugation to primary amine groups.[38] The 15-mer peptide GSGAAAGLS$(His)_6$ was labeled on the unique N-terminal primary amine with excess NCS-activated Os complex and purified as described in the Methods; see Figure 1A.

Similar to the peptides used in many of our previous reports, this sequence is modular in nature, with each module providing a different intended utility. The N-terminal amine functions as a unique site for covalent attachment of the Os complex. GAAAG is an intervening spacer or linker consisting of an Ala-helix that is broken by the Gly residues. The Leu and Ser residues are meant to provide some rotational flexibility, while the C-terminal $(His)_6$ motif allows

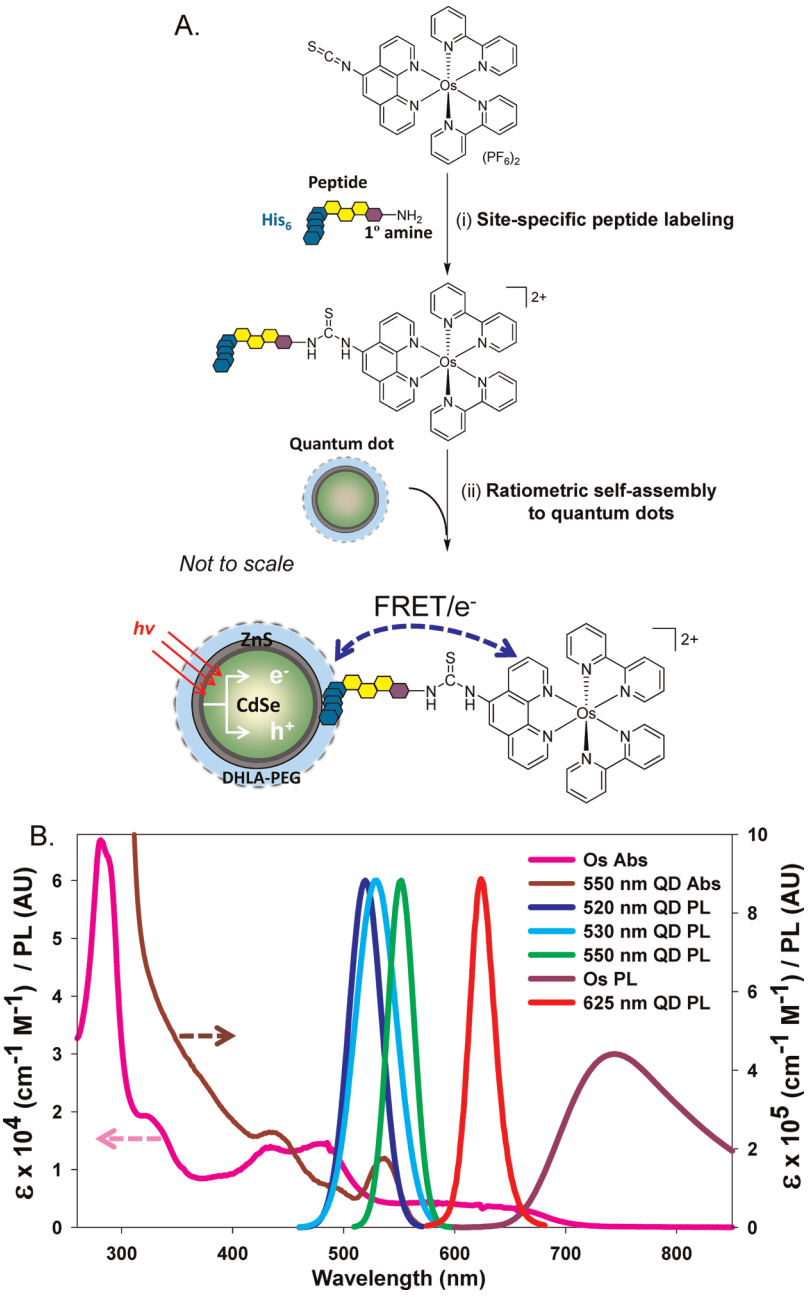

Figure 1. Synthesis and self-assembly of QD−osmium conjugates. (A) Step 1: the unique primary amine on the peptide is site-specifically modified with osmium isothiocyanate complex. Step 2: Os-pep is ratiometrically self-assembled to the surface of DHLA-PEG-coated QDs *via* the $(His)_6$ sequence. Schematic of QD self-assembled with one Os-pep. Photoexcitation of the system may result in PL quenching of the QD *via* FRET or an alternative electron transfer pathway. (B) Spectral overlap: selected absorption and emission spectra of the four QD samples and the Os-pep. Note: only 550 nm QD absorbance shown for brevity.

for conjugation of the labeled peptide to the QD. In conjunction with the poly(ethylene glycol)-appended dihydrolipoic acid (DHLA-PEG; see Methods) surface ligands, the small linker length should afford the Os-bpy label excellent proximity to the QD while still extending it away from the surface sufficiently to prevent potential contact-based quenching. This metal affinity coordination interaction arises between the histidine's pendant imidazolium side-chain groups and the Zn on the QD surface and is characterized by a rapid assembly (seconds) based on a high intrinsic avidity ($K_d^{-1} \approx 10^9$ M^{-1}). Conjugation itself is facile to implement, as all it requires is mixing of both participants while still providing intimate control over the ratio of peptide displayed per QD.[6,39] Recent work has shown that DHLA-capped QDs can controllably display valences ranging from 1 to 50 ± 10 peptides using such an assembly approach.[40] Overall, the peptide sequence is intended to provide a physical

TABLE 1. Selected Photophysical Properties of the QD−Os Systems

QD donor with Os-bpy	quantum yield[a]	overlap integral $J(\lambda) \times 10^{-14}$ (cm^3/M)	Förster distance R_0 (Å)	QD radius (Å)	separation distances r (Å)	
					predicted	experimental
520 nm	0.20	4.40	34.2	26	38	35.6
530 nm	0.22	4.16	34.4	29	41	48.5
550 nm	0.19	3.80	33.1	30	42	51.3
625 nm	0.80	5.33	44.5	50	63	64.9
(Os-bpy)[c]	0.005[b]	0.69	13.6			

[a] Determined by comparison to dye standards. [b] Quantum yield at 745 nm. [c] Os-bpy-labeled peptide: molar ext coeff 12 500 M^{-1} cm^{-1} at 490 nm.

bridge for attaching the Os complex to the QDs in a stoichiometric manner, which affords us the ability to carefully control and analyze the subsequent interactions.

Figure 1B shows the absorption and emission spectra of the Os-labeled peptide and the four QD samples (520, 530, 550, and 625 nm emitting) utilized in this study (Note: Os-pep refers to the labeled peptide hereafter, while Os and Os-bpy refer to the attached metal complex itself). The Os-pep displays an almost insignificant quantum yield (QY) of 0.5% with a phosphorescent emission centered at ~745 nm; this is followed by a long red tail that continues well into the near-IR. The Os-pep absorption spectrum displays the numerous metal-to-ligand charge transfer (MLCT) transitions expected for such coordinated metal molecules, and the cumulative effect of these is to also extend the absorbance beyond 700 nm.[41,42] The wide Os-pep absorption spectrum also results in a low spectral overlap with the four Gaussian-shaped QD PL profiles. As highlighted in Figure 1B, spectral overlap between each QD PL profile and the Os absorption is rather modest. Reinforcing this point, the QD absorption scale is an order of magnitude larger than that of the Os-pep. Within the area of spectral overlap, the Os-pep extinction coefficient drops from 12 500 M^{-1} cm^{-1} at 490 nm to ~3500 M^{-1} cm^{-1} at 570 nm, yielding relatively small overlap integrals with corresponding Förster distances (R_0) centered around a range of 33 to ~34 Å (Table 1), except for the 625 nm QDs (*vide infra*). This is in dramatic contrast to the spectral overlap for a similar set of QD donors (510, 530, and 555 nm PL maxima, similar QYs) when paired with a Cy3 dye acceptor.[43] There the spectral overlap integrals were 10-fold larger and the Förster distances increased significantly to a ~48−57 Å range. These differences are directly attributable to the Cy3 extinction coefficient, which is around 12 times larger in the same portion of the spectrum (150 000 M^{-1} cm^{-1} at λ_{emmax} = 555 nm). For the 625 nm QDs, the Os-pep extinction coefficient drops to a paltry ~2600 M^{-1} cm^{-1} at 625 nm; however, this is more than compensated for by the remarkably high QD donor QY of 80%, which is almost 4 times that of the other QD samples. This leads to an overlap integral of 5.33 × 10^{-14} cm^3/M, which is ~20% larger than that of the next highest value for the 520 nm QD−Os interaction, and an estimated R_0 of 44.5 Å, which is also 10 Å larger (30%) than any other predicted value in Table 1. We also note that for any homoFRET interactions the Os-bpy label has a predicted Förster distance of 13.6 Å and a correspondingly small overlap integral of ~0.7 × 10^{-14} cm^3/M.

Steady-State Fluorescence Analysis. We began by self-assembling increasing ratios of Os-pep onto each of the QD samples and examining the resulting spectral changes. Figure 2A,B shows representative steady-state PL spectra collected from the 530 and 550 nm emitting QDs, respectively, when assembled with the indicated evolution of increasing Os-pep ratios (n = 2−30, excitation 350 nm). Figure 2C shows a comparative summation plot of the decrease in QD PL *versus* Os-pep ratios for 520, 530, and the 550 nm QDs (spectra for the 520 nm QDs can be found in the Supporting Information). All three samples display a similar strong quenching response to the presence of increased Os-pep. The 520 nm QDs are almost completely quenched at a ratio of 12 Os-pep/QD, while the 530 nm QDs retain ~20% of their initial PL at 30 Os-pep/QD. In contrast, the 550 nm QDs retained almost 30% of their PL even when the Os-pep valence was increased to a maximum of 30. This indicates that quenching is not uniform for these differentially emissive QD samples, and indeed similar trends have been noted with other sets of QD samples for both QD-FRET and electron transfer to/or from the QD.[19,20,43] The quenching data were then subjected to analysis using eqs 4−6 as described in the Methods. This is based on a Förster framework that describes QD donor resonance energy transfer (RET) with n acceptors placed at a fixed separation distance r around the QD surface. The corresponding normalized FRET efficiency E for this QD-conjugate data series is shown in Figure 2C, inset. We also utilized FRET E corrected (see Methods) as a mechanism to probe the uniformity of the underlying assembly process by looking for significant deviations in expected quenching kinetics. These would arise from heterogeneous QD−peptide ratios especially at low valence.[44] The ≤10% deviations observed, however, suggest that this was not a significant issue here (data not shown).

The most efficient putative FRET is observed for the 520 nm QDs with a FRET E approaching 96% at a

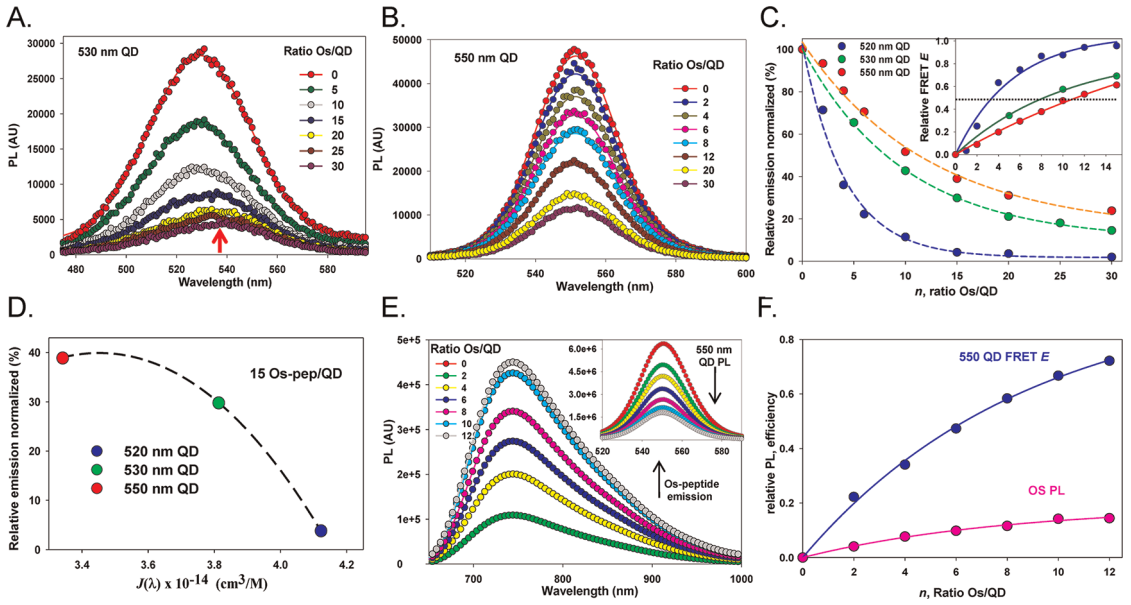

Figure 2. Steady-state photoluminescence spectra. Representative PL spectra collected from (A) 530 nm and (B) 550 nm emitting QDs assembled with the indicated increasing ratios of Os-pep in PBS. The red arrow in A highlights the asymmetric QD quenching. (C) Comparison of the normalized quenching of 520 nm (blue), 530 nm (green), and 550 nm (red) QDs when assembled with increasing ratios of Os-pep. FRET *E* for 520, 530, and 550 nm emitting QDs *vs* assembled Os-pep ratio is shown in inset. (D) Normalized emission of the same QDs as a function of spectral overlap $J(\lambda)$ for a nominal valence of 15 peptides. (E) Representative, deconvoluted PL spectra collected from sensitized Os-pep acceptor following self-assembly of the indicated increasing ratios of $(His)_6$-peptide-Os onto 550 nm QD donors. Inset: corresponding 550 nm QD PL quenching. (F) Plot of FRET *E* (blue) and corresponding sensitized Os emission (pink) as a function of Os-pep/QD valence from the data in E. 520 nm QD quenching data and plots of QD PL loss *vs* FRET *E* for 520, 530, and 550 nm QDs can be found in Supporting Figure 2.

valence ≥ 15 Os-pep/QD. The 530 and 550 nm QDs approach efficiencies of ~69% and 61%, respectively, at the same valence. This trend reflects that the highest FRET *E* (or QD PL loss) corresponds to the smallest QD (520 nm emission) and progressively decreases as the QD emission maxima become longer (larger QDs) and donor–acceptor spectral overlap decreases. Further examination of Figure 2C, inset, reveals that for each QD conjugate the point where FRET $E \cong 50\%$, indicated with the black dashed line, shifts significantly to a higher ratio *n* of Os/QD as a function of increasingly red QD PL emission. As an alternate way to view the same data, we plot relative emission for each QD color at a median ratio of 15 Os/QD *versus* their spectral overlap function $J(\lambda)$ with Os in Figure 2D; see also Table 1. Increases in QD quenching and spectral overlap clearly track each other at the same Os valence values.

Analysis of the FRET *E* data with eqs 5 and 6 yielded the experimental QD donor to Os acceptor center-to-center separation distances (*r*) listed in Table 1. These increased from ~36 Å for the smallest 520 nm QDs to ~51 Å for the largest 550 nm QDs in this set. In comparison, the predicted values are in the 38 to ~42 Å range. These values are arrived at by considering the predicted QD core–shell size (radius ~26, 29, 30 Å, respectively)[45] with a nominal peptide contribution of ~12 Å, assuming that the $(His)_6$ is fully coordinated to the QD surface and does not contribute any significant extension,[46] a simple linear extension of ≤12 Å for the central linker portion of the peptide, and that the Os linkage and polypyridyl structural radius also have a minimal contribution of ≤3 Å. It is important to note that these are only predicted values made by assuming simple linear structures. In reality, the peptide structure on the QD can assume a variety of different conformations due to both flexibility and a wide degree of rotational freedom, as recently shown for structurally similar QD-peptido-DNA constructs.[47] The predicted and experimental values are quite close for the smallest 520 nm QDs (38 and 35.6 Å, respectively) with only a ~3 Å (−10%) to (<10%) difference. This experimental separation value is also only ~1.4 Å larger than the calculated R_0 of 34.2 Å. The two larger QDs demonstrate a much larger deviation of ~7.5 and 9 Å (~15–20%).

The excellent fit of the quenching data (Figure 2C) to a nominal sixth-power dependence expected for a FRET process along with the QD size/emission-dependent quenching and spectral overlap trends observed in Figure 2D led us to probe the steady-state Os-pep emission in this same QD-assembled configuration. As this was subsequent to the data collected in Figure 2A–D, we utilized a slightly different hydrophilic 550 nm QD sample, the principle difference being a slightly broader full-width at half-maximum PL spectra. More importantly, the representative deconvoluted Os-pep emission spectra plotted in Figure 2E show that as 550 nm QD PL is similarly quenched by increasing Os-pep valence (inset), the corresponding sensitized Os emission increases in a manner that directly

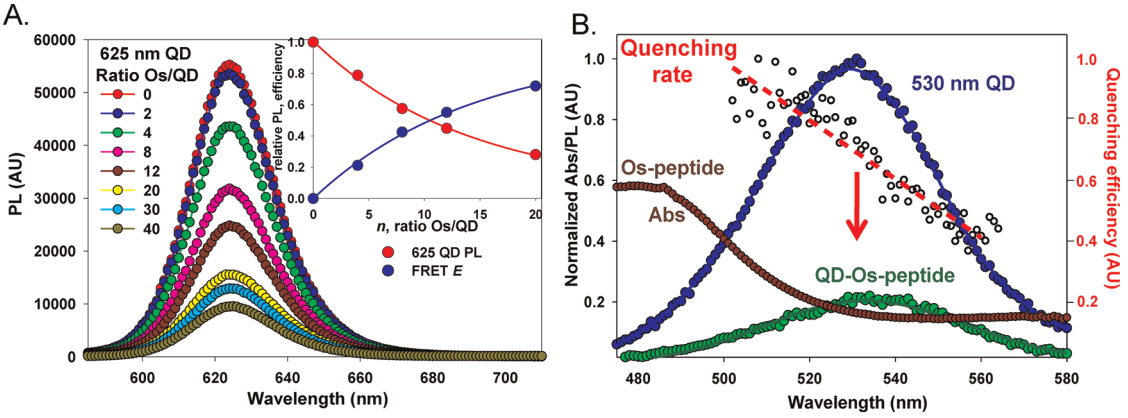

Figure 3. 625 nm QD interactions and wavelength-dependent FRET analysis. (A) Representative PL spectra collected from 625 nm emitting QDs assembled with the indicated increasing ratios of Os-pep in PBS. Inset plots the QD donor loss (red) and FRET *E* (blue) as a function of Os-pep/QD ratio in this sample. (B) Normalized PL spectra from 530 nm QDs in the absence of Os-pep (blue) and when assembled with 25 Os-pep (green) along with the normalized Os-pep absorption (brown). Individual points making up the wavelength-dependent FRET quenching rate calculated from 500 to 560 nm are shown (black) with a line of best fit (red).

tracks the assembly valence. This datum plots only the sensitized Os emission component, as the directly excited contribution was estimated and subtracted by monitoring Os-pep only controls at the same concentration range within the same excitation regime; these contributions ranged from essentially negligible to approximately 30% at the highest valence of 12. The changes in magnitude of the emission intensity between each of the spectra (*i.e.*, changes in Os-pep sensitization relative to QD PL loss, inset shown in Figure 2E) track each other reasonably well. However, the difference in overall emission intensities is quite striking, as Os-pep luminescence is an order of magnitude smaller than the QD PL; see also Supporting Figure S3 for the unprocessed data. The low rate of sensitized Os complex emission is directly attributable to its extremely low QY (~0.5%). Figure 2F plots the rate of FRET *E* in this configuration *versus* the increases in Os-pep sensitization as a function of acceptor valence. Clearly, FRET *E* and Os-sensitization increase in a similar manner as peptide-valence changes around the QD.

Given the results for the above three QD samples, we opted to probe the interactions of a 625 nm QD sample displaying a more red-shifted emission to verify if quenching could be extended to samples where spectral overlap should be significantly smaller. Figure 3A shows representative data collected from the 625 nm QDs when assembled with increasing ratios of Os-pep. The inset in this figure plots the corresponding normalized QD PL loss and FRET *E* for this data set. Similar to the data described above for Os interactions with the 520−550 nm QD samples, these QDs are also strongly quenched in the presence of increased Os-pep, with 50% quenching observed at a valence of ~12 peptides, which increases to 80% at a ratio of 40. Although the Os-bpy absorption in this part of the spectrum is ≤75% of that for the 500−560 nm range, this is more than compensated for by the extremely high QY of this QD sample (~80%). This means that the point where FRET *E* reaches ~50% does not continue the trend displayed by the other three QD samples (see Figure 2C, inset). Analysis of this FRET data yields an experimental separation distance (*r*) of 64.9 Å, which is only ~2 Å larger (3%) than the predicted value of 63 Å. The much larger separation distance, in this case, is directly attributable to the significantly larger diameter of 10 ± 1 nm estimated for these redder QDs.

Wavelength-Dependent FRET Analysis. Some asymmetrical features were noted in the steady-state PL spectra collected from QDs conjugated to higher valences of Os-pep. These were especially evident in Figure 2A at ratios of 10 peptides and higher, where a noticeable red-shift in the 530 nm QD PL maxima can be observed (see red arrow). PL spectra of QD solutions are typically characterized by a relatively narrow Gaussian appearance that represents a narrow distribution of QD sizes. This spectrum is, in turn, a composite spectrum made up of much narrower bands that are associated with well-defined, discrete QD sizes.[48] Previous work has shown that the individual QD emitters (QDs of different size and PL maxima) within such a macroscopic QD sample display discrete overlap integrals $J(\lambda)$ and ET rates in a FRET configuration that depend directly on the corresponding acceptor's absorption profile.[48] More pertinently, a spectrally dependent FRET rate can be derived from the quenched ensemble QD PL in this configuration. We subjected spectra collected from the 530 nm QD−Os peptide assemblies to this analysis using eqs 7 and 8 as described in the Methods.

Figure 3B presents representative results of this spectrally dependent FRET analysis. The normalized PL spectra from 530 nm QDs in the absence of Os-pep are shown in blue; corresponding data collected from the same QDs conjugated with 25 Os-pep are shown in green along with the normalized Os-pep absorption in

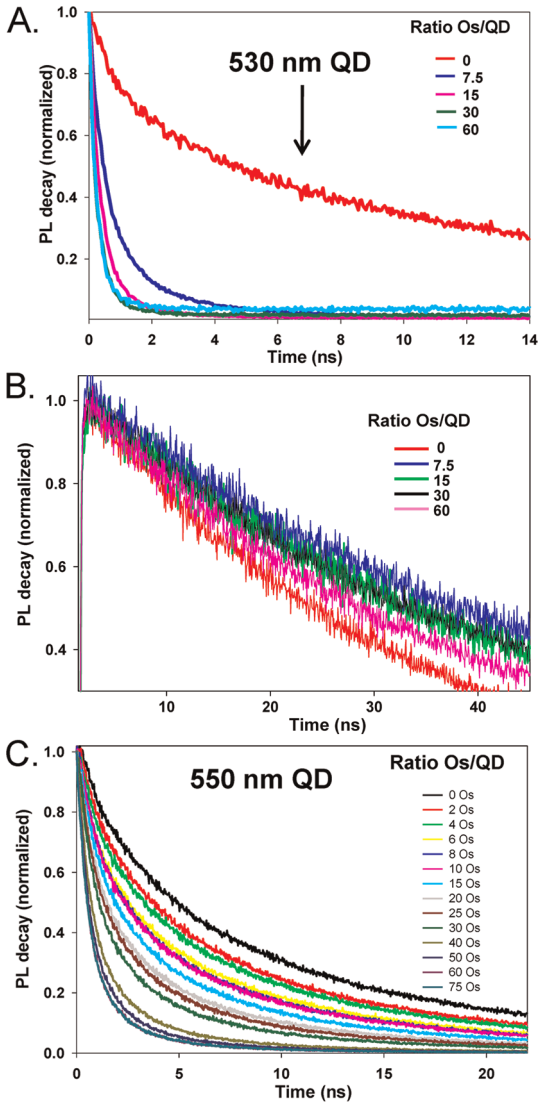

Figure 4. Excited-state lifetimes. Representative, normalized time-resolved PL decays from the 530 nm emitting QD donors (A) and Os-pep acceptors (B) collected from QD−Os conjugates with the indicated increasing ratios of Os-pep per QD. (C) Normalized time-resolved PL decay data collected from 550 nm emitting QDs assembled with the indicated ratios of Os-pep.

brown. The individual points making up the wavelength-dependent FRET quenching rate, calculated over the 500−560 nm portion of the spectral window, are shown in black with a line of best fit to the data superimposed in red. This particular range was utilized, as it encompasses the majority of the QD PL profile, namely, 530 nm QD emission maxima ± 30 nm. The analysis confirms that QD quenching is indeed wavelength-dependent, as the rate of quenching directly tracks the underlying spectral overlap for this particular QD donor−acceptor FRET pair. In contrast, uniform-flat, wavelength-independent rates of QD quenching were observed for QDs interacting with gold nanoparticles or the aforementioned electron-donating Ru(II) phenanthroline compound when interacting *via* non-FRET processes.[13,20]

Excited-State Lifetime Analysis. To complement the steady-state analysis, we subjected the QD−Os-pep assemblies to fluorescence lifetime analysis. Figure 4A shows normalized time-resolved PL decays from 530 nm QDs assembled with Os-pep ratios ranging from 7.5 to 60 in increments that double; the highest valence is used to ensure saturation of the QD surface. QD decays were fit to a biexponential function, and the corresponding average lifetimes (τ_{av}) and individual lifetime components ($\tau_{1,2}$) along with their fractional amplitudes are presented in Table 2. The excited-state QD lifetime decreases significantly (~85%) in the presence of Os-pep, going from a τ_{av} of 14.1 to 2.13 ns when assembled with an average of just 7.5 peptides. Lifetimes continue to decrease with increasing Os valence, reaching a value of 0.51 ns (~97% quenching) at approximately 60 peptides/QD. These decay trends parallel the corresponding steady-state data in Figure 2B and E, where almost complete quenching was observed at ≥30 Os-pep per 530 nm QD.

Corresponding sensitized lifetimes of Os-pep when assembled on the QDs were also examined. Figure 4B shows the Os emission collected from the same assemblies at the same time. The lifetime values from fitting these decay profiles with a monoexponential

TABLE 2. Lifetimes of 530 nm QDs and Os-Peptide at Selected Conjugate Ratios

	lifetime (ns)			
	530 nm QD[a]			Os-peptide[b]
ratio of Os-peptide/QD	τ_{av} (% quenching)	τ_1	τ_2	τ
0	14.1 (0)	14.90 ± 0.11 (70.4%)	2.20 ± 0.16 (29.6%)	30.8 ± 0.28
7.5	2.13 (85)	2.87 ± 0.03 (31.7%)	0.69 ± 0.01 (68.3%)	53.2 ± 0.65
15	0.97 (93)	1.36 ± 0.02 (28.8%)	0.40 ± 0.01 (70.2%)	50.7 ± 0.69
30	0.58 (96)	0.90 ± 0.03 (21.8%)	0.26 ± 0.01 (78.2%)	45.7 ± 0.52
60	0.51 (97)	0.67 ± 0.03 (34.5%)	0.18 ± 0.01 (65.5%)	38.6 ± 0.40

[a] Amplitude weighted as described and fitted with a biexponential function. Both lifetime components are given along with their fractional intensity. [b] Fitted with a monoexponential function.

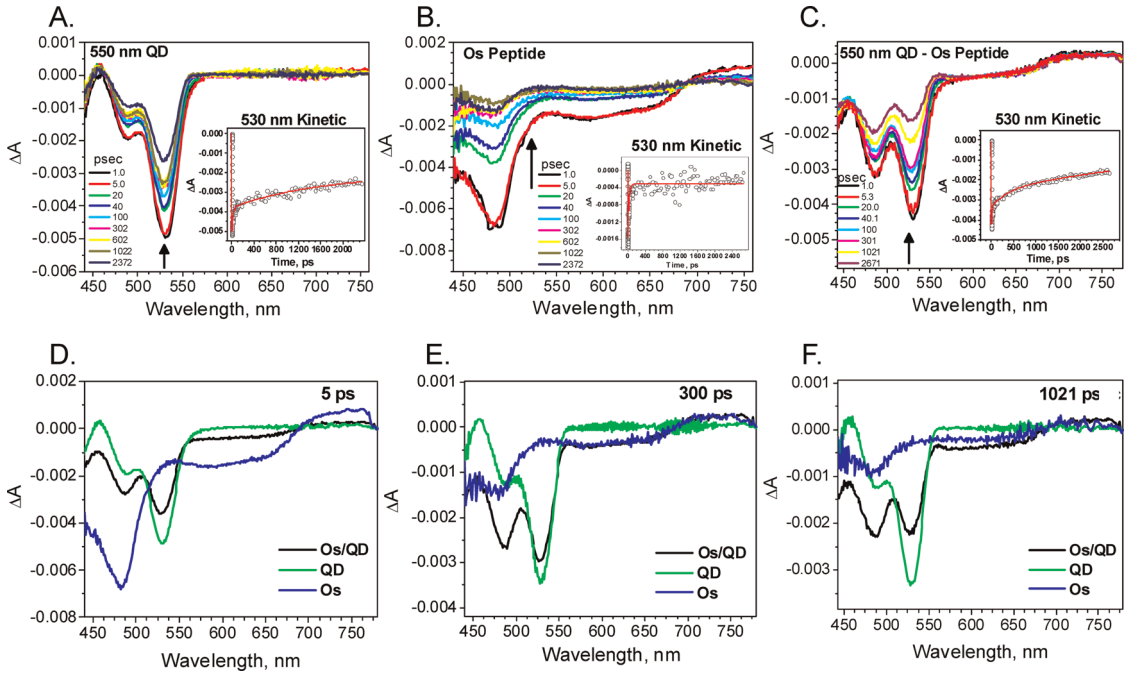

Figure 5. Transient absorption spectra. (A–C) Transient absorption spectra of 550 nm QDs (A), Os-pep (B), and 550 nm QD–Os conjugates (40 Os/QD) (C) at selected times, excited at 415 nm. Insets: Corresponding time-resolved transient absorption data monitored at 530 nm, experimental data (circles) and best fit (red line). (D–F) Superimposed transient absorption spectra of Os-pep (blue), QD (green), and QD–Os conjugates (black) at 5 ps (D), 300 ps (E), and 1021 ps (F) excited at 415 nm.

function are also presented in Table 2. Interestingly, the sensitized Os-pep lifetime demonstrates a significant ~40% increase from 30.8 to 53.2 ns when assembled on the QDs at the lowest 7.5 ratio. This value then gradually decreases to ~38.6 ns at the highest ratio, although this is still higher than the native unsensitized lifetime. A similar pattern of behavior (steady state: decrease in QD donor PL and increases in acceptor sensitization/excited-state: decreases in QD donor lifetime and initial increase followed by *decreasing* acceptor sensitization as acceptor valence increases around the QD) has been noted for other QD assemblies including those using organic dyes and an mCherry fluorescent protein.[43,46]

Figure 4C shows normalized time-resolved PL decays collected from 550 nm QDs assembled with ratios from 2 up to 75 Os-pep/QD. Again, the highest valence is used to ensure saturation of the QD surface. The corresponding τ_{av} and individual lifetime components along with their fractional amplitudes are presented in Supporting Table 2. The QD lifetime decreases 37% from an average of 10.41 ns to 6.61 ns when assembled with 8 peptides. Similarly, average lifetimes continue to decrease with increasing Os valence, reaching a value of 1.4 ns (~86% decrease) at nominal surface saturation. These decay trends also parallel the corresponding steady-state data in Figure 2C, where ~80% quenching was observed at ≥30 Os-pep per QD. The decrease in relative quenching rate, in comparison to that observed for the 530 nm QD donor lifetimes examined above, may reflect the smaller spectral overlap and increased QD size, which combine to lower the overall probability of intra-assembly FRET.

Transient Absorption Spectroscopy. Femtosecond transient absorption (FSTA) experiments were performed on 550 nm QDs, free Os-pep, and the full QD–Os-pep assembly (valence of 40) to provide insight into the ET processes within the conjugates. As shown in Figure 5A, photoexcitation of 0.5 μM 550 nm QDs at 415 nm with 150 fs laser pulses resulted in ground-state bleaching features at 480 and 530 nm, corresponding to the QD's lowest energy transitions. The ground-state bleach, arising from an electron being promoted from the QD valence band to the conduction band, displays a fast rise time within the 200 fs instrument response time. Over the time range examined, the ground-state recovery kinetics monitored at 530 nm are biexponential with a fast recovery of 22 ± 2 ps (42%), attributed to the direct electron–hole recombination, and a slow 1.5 ± 1.0 ns (56%) component that persists on the nanosecond time scale; see Figure 5A, inset. This longer lifetime component follows the excited-state lifetime of the 550 nm QD and is partially attributable to carrier trapping at localized surface defect states.[49,50] This component may also be attributable to exciton thermalization from the optically active $F = 1$ to the optically passive $F = 2$ dark state and is consistent with results observed in early time-dependent experiments on CdSe NCs.[51,52] Kinetics monitored at 488 nm also exhibit biexponential behavior similar to the measured rates at 530 nm (Supporting Figure S5).

Photoexcitation of a 100 μM Os-pep sample at 415 nm into the ^{1}MLCT proceeds through rapid intersystem crossing to the ^{3}MLCT to form $[Os^{3+}(phen)(bpy)(bpy^-)]^{2+}$ within 300 fs. A biexponential ground-state recovery at 488 nm of 20 $\pm$ 0.2 ps (85%) and 439 $\pm$ 3.0 ps (12%) with a long-lived ΔA that persists on to the nanosecond time scale was observed (Figure 5B and Figure S3). Time-resolved fluorescence measurements on free Os-pep reveal a ^{3}MLCT lifetime of ~31 ns (Table 2). The kinetics signal obtained at 530 nm, shown in Figure 5B, inset, is weaker than that of the 550 nm QD and exhibits fast, 2.0 $\pm$ 0.5 ps (11%), and slower, 26 $\pm$ 2 ps (89%), decay components.

Excitation of the full QD–Os-pep assembly (valence: 40) at 415 nm results in a strong ground-state bleach within 1 ps in the 450 to 550 nm portion of the spectra. This encompasses both QD ground-state bleach features at 530 and 480 nm and the Os-pep bleach at 488 nm. The corresponding kinetics monitored at the peak of the QD bleach, 530 nm (Figure 5C, inset), are triexponential in this case, with τ_1 = 14 $\pm$ 0.3 ps (22%), τ_2 = 322 $\pm$ 2 ps (59%), and τ_3 = 5 $\pm$ 2 ns (19%). The kinetics at 488 nm, corresponding to the peak of the Os-pep bleach, is shown in Supporting Figure S5. For comparison purposes, overlapping ground-state spectral features of the QD, Os-pep, and QD–Os-pep conjugate spectra were plotted at 5 ps, 300 ps, and 1 ns and are shown in Figure 5D–F. Clearly, the spectral features of the QD and Os-pep alone are different from that of the QD–peptide-Os conjugate. Within 5 ps, ground-state bleaches at 488 and 530 nm are observed and are comprised of both QD and Os-pep absorption features. By 300 ps, the Os-pep bleach feature at 488 nm is dramatically reduced, while the 530 and 480 nm features associated with the 550 nm QD are reduced by only ~20%. Significant changes occur in the bleaching spectra of the QD–Os-pep complex between 5 and 1021 ps. The intensity of the 488 nm bleach band increases with respect to the 530 nm band, having nearly equal intensities by 300 ps and then surpassing the 530 nm band intensity by 1021 ps. The relative growth of the 488 nm feature and its persistence over time, as seen in Figure 5D–F, is the result of excitation of the Os-pep complex *via* FRET from the 550 nm QD.

DISCUSSION AND CONCLUSIONS

Investigations with several structurally similar Os(II) polypyridyl complexes that functioned either as quenchers/acceptors in electron transfer systems or as photoinduced electron donors for TiO_2 and ZrO_2 semiconductor nanoparticles led us to investigate their interactions with CdSe/ZnS QDs.[29–33] Although not fully detailed therein, these systems also displayed some underlying characteristics and spectral overlap that were quite similar to ours. We began by estimating the relative QD and Os-bpy energy levels. Literature and experimental values for the reduction (E_{Red} ≈ −1.00 V *vs* Ag/AgCl [3 M KCl]) and oxidation (E_{Ox} ≈ 1.45 V *vs* Ag/AgCl [3 M KCl]) potential of CdSe/ZnS QDs (assuming a core diameter of 2.2 nm with ~3.5 layers of ZnS) were used to estimate the electron affinity (E_a) and ionization potential (I_p): conduction band and valence band energy levels, respectively.[53–55] These values originate from electrochemical measurements of CdSe/ZnS QDs and are not significantly different from those previously used for CdSe core-only QDs.[20,53–55] Similarly, the I_p for the Os-pep was calculated from the experimentally determined oxidation potential (Supporting Figure S6), while the E_a was estimated from a combination of the I_p and the absorption onset.[56] Examining the overall QD–Os-bpy spectra (Figure 1B) in conjunction with the relative energy levels (see Figure 6A) led us to predict two alternate ET processes as being possible for quenching of QD PL in the paired QD/Os-bpy system.

The first ET process we consider is FRET from the photoexcited QD donor to the Os-bpy acceptor arrayed around its surface (I. FRET). The photoexcited QD transfers energy to the Os-bpy acceptor *via* dipole–dipole Förster coupling, which results in quenching of QD PL and a sensitized Os-bpy emission. Our principal concern for this scenario was the extremely low Os-bpy extinction coefficient, which gives rise to a small spectral overlap with the QDs. The second process is based on CT (II. Charge Transfer), where the directly photoexcited Os-bpy, with its significantly longer lifetime, is able to transfer an electron to the QD. Given the relative energy levels discussed above, CT in the other direction (*i.e.*, QD-to-Os) is not favorable, but cannot be unambiguously ruled out. Both FRET and CT efficiencies are highly distance dependent. FRET follows a $1/r^6$ dependence and is governed by the donor fluorescence quantum yield and donor–acceptor dipole–dipole interactions, which are determined by the spectral overlap between the luminescence and absorption bands of the donor and acceptor, respectively. Electron transfer, *via* superexchange, decays exponentially with distance, but is dependent on an underlying favorable driving force, ΔG, for charge transport between the donor and acceptor. At large distances (>10 nm), electron transfer is expected to proceed at a much slower rate than FRET; however, this has not been studied systematically for QD systems. At shorter distances (≤10 nm), both processes are expected to be fast, and it still remains somewhat unclear how both would compete.[35,57,58] We do not consider QD quenching by the heavy metal proximity effect, as that would have manifested a linear quenching response typically characterized by a Stern–Volmer function and would also not yield Os sensitization.[59] We also do not consider a Dexter ET mechanism given the donor–acceptor separation distances, which should preclude this.[60] In the following, we discuss the

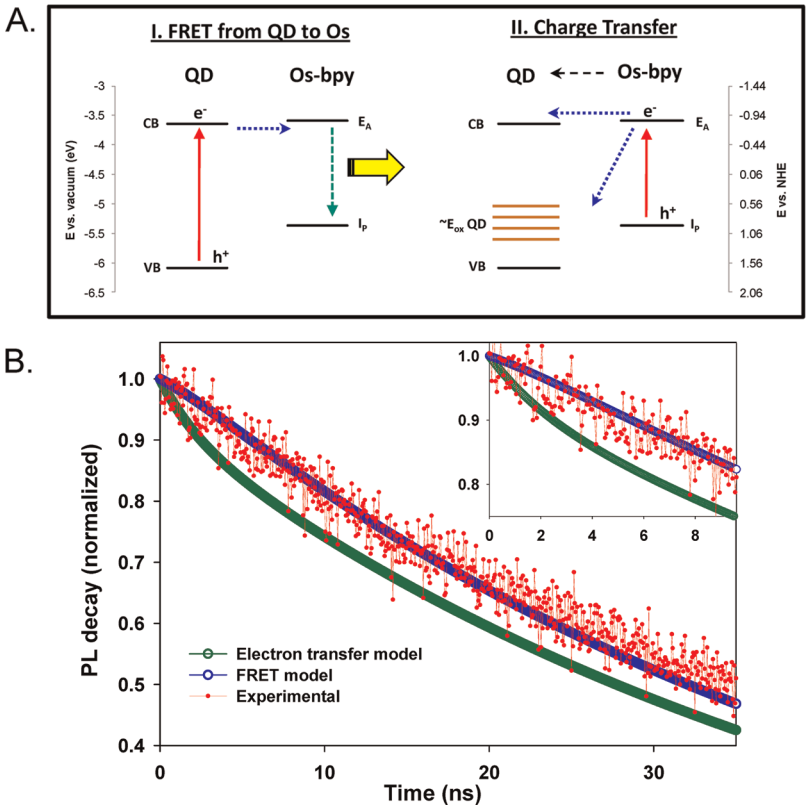

Figure 6. Schematic representation of possible energy transfer pathways. (A) (I) FRET consists of dipole−dipole Förster coupling from the photoexcited QD donor to the Os-bpy acceptor arrayed around its surface. In this case, the QD is photoexcited by incident light and transfers energy to the Os-bpy acceptor, which results in a sensitized emission. (II) Charge transfer. The second process is based on CT. Following photoexcitation, the excited Os-bpy, with its longer native lifetime, is able to transfer an electron to the relaxed QD. (B) Modeled Os-bpy decay profiles at a nominal valence of 7.5/QD assuming either FRET sensitization by the QD or electron transfer to the QD. The normalized experimental data collected at the same valence is superimposed in red. Inset highlights the first ~10 ns.

evidence for and against each of the two putative processes in the context of the experimental data.

Clearly, there is significant evidence supporting a QD FRET process and arguing against CT. Although relatively small in comparison to pairing QD donors with organic dye and fluorescent protein acceptors,[43,46] reasonable spectral overlap still exists between the QD and the Os-bpy (Figure 1B, Table 1). The short peptidyl linker used here is predicted to place the Os-bpy acceptor at a distance ~12 Å from the QD surface, although our data reflect an average of 16 ± 5 Å. This is equivalent to placing the acceptor at a distance of R_0 plus an additional 5 to 13 Å away from the QD center; see Table 1. Even with experimentally derived distances varying somewhat from predictions, given the R_0 values ranging from ~33 to 45 Å, this more than satisfies the donor−acceptor $R_0 \pm 0.5R_0$ separation "rule of thumb" where efficient FRET can be expected for most donor−acceptor pairs.[61,62] Steady-state PL spectra collected from complexes assembled with increasing ratios of Os-pep/QD show QD donor PL quenching in conjunction with a small sensitization of the Os-bpy acceptor (Figure 2). Moreover, increases in the rate of quenching and sensitization directly track increases in assembled Os-pep valence, while quenching also decreased as a function of spectral overlap. These results mirror similar trends noted for QD donors when paired with increasing QD/acceptor ratios of fluorescent FRET acceptors.[9,43,46] One further and critical piece of evidence supporting a FRET interaction was obtained from the wavelength-dependent quenching analysis (Figure 3), demonstrating that the QD quenching rate is indeed a direct function of the underlying spectral overlap.

Analysis of the excited-state lifetime results corroborate the data collected in the steady-state format, that is, significant QD donor quenching along with some acceptor sensitization, with both, again, tracking Os-pep assembly valence (Figure 4). In combination with estimates of direct Os-bpy excitation as its conjugate valence increases (see Table 3 and below), we note that all QD samples undergo significant quenching at valences of less than 7−8, where direct excitation of surrounding Os in the conjugates is less than 20% that of the QD excitation. The lifetime data (Figure 4, Table 2) were used to extract relevant ET rates, which are presented in Table 3. The normalized ET rate per QD−Os pair is estimated to be 0.053 ns^{-1} for an Os-bpy acceptor valence of 7.5. This increases to 0.064 ns^{-1} when the Os-bpy ratio increases to 15 and

TABLE 3. Relative Absorption and Estimated Energy Transfer Rates

ratio of Os-peptide/QD (n)	rel abs Os-bpy[a]	rel abs QD[a]	k_{ET} (ns^{-1})	$(1/n)k_{ET}$
0	0	1.0		
7.5	0.16	0.84	0.40	0.053
15	0.27	0.73	0.96	0.064
30	0.43	0.57	1.65	0.055
60	0.60	0.40	1.88	0.031

[a] Rel abs = $\varepsilon_{Os\text{-}bpy}/\varepsilon_{Os\text{-}bpy} + \varepsilon_{QD}$ (Os-bpy $\varepsilon_{375nm} = 7667$, 530 nm QD $\varepsilon_{375nm} = 302\,690$).

then drops to 0.055 and 0.031 ns^{-1} when acceptor ratio increases to 30 and 60, respectively. The averaged normalized rates for the valences of 7.5, 15, and 30 Os acceptors per QD are quite similar and are centered around 0.057 $\pm$ 0.006 ns^{-1}. Estimates of the relative absorption by Os-bpy and the 530 nm QD at 375 nm are shown in Table 3. Within a single QD–Os-bpy complex, it is highly unlikely that both a QD and an Os-bpy will be excited based on the relative numbers of photons per pulse ($\sim 10^7$) and the number of complexes present in the excitation volume ($\sim 10^{12}$). Therefore we only need to consider processes that involve an excited-state QD and ground-state Os-bpy complexes or a ground-state QD and an excited-state Os-bpy. At a ratio of 7.5 Os/QD, we estimate that about 16% of the absorbed photons will excite Os-bpy directly and the remaining 84% of the absorbed photons excite the QDs. The excited QDs are efficiently (85%) quenched by the ground-state Os-bpy complexes, leading to the observed sensitized emission. Both the directly excited and sensitized Os-bpy contributes to the fluorescence signal. Direct Os-bpy excitation increases to 28% at a ratio of 15, where almost full quenching of the QD ($\sim$93%) is seen. As the number of Os-bpy arrayed around the QD continues to increase, their relative rate of excitation increases to $\sim$60% at a valence of 60, while the QD quenching efficiency approaches 97%. The normalized ET rate for a valence of 60 is significantly lower than for the lesser valences and may reflect saturation effects as the ET efficiency approaches 1. FRET from the Os-bpy to the QD is not an available pathway due to the complete lack of spectral overlap. For comparison purposes, similar 530 nm QDs (QY $\sim$0.2) demonstrated a rate of 0.13 ns^{-1} when interacting with four surrounding DNA assembled Cy3 acceptors.[47] This normalizes to approximately 0.033 ns^{-1} for a single QD-single-Cy3 acceptor, a value not radically different from those estimated here for QD–Os-bpy interactions.

The FSTA data also support a FRET mechanism. First, the ground-state spectra of the Os–QD match closely with a combination of both the QD and Os spectra, indicating that a significant population of both ^{3}*Os and *QD are formed within several picoseconds. Examination of the relative bleach intensities of the Os-bpy at 475 nm and the 550 nm QD feature at 530 nm in the QD–Os-bpy complex in Figure 5 reveals a distinct increase in the Os-bpy ground-state bleach feature over time, relative to the 550 nm QD. On the basis of the fluorescence lifetime data, the 550 nm QD is efficiently quenched on a time scale of $\sim$1 ns. This is the exact behavior expected if FRET were the primary mechanism for QD quenching. Additionally, no direct observation of the oxidized or reduced Os complex was noted in the FSTA spectra. Lastly, examination of the differential QD absorption spectra in the absence and presence of increasing Os-pep (Supporting Figure S4) showed no bleaching of the QD absorption features. This would have been indicative of CT from the metal to the QD, as noted for CdSe/ZnS QD interactions with Ru(II) phenanthroline assembled using similar peptide bridges.[20]

Although the evidence for QD FRET quenching by the Os-bpy is strong, not all the data directly support this mechanism. We note several items that are somewhat incongruous or that would be expected for a CT process. The first is that, in all cases, QD PL quenching efficiency directly tracks the ratio of Os-bpy brought into close proximity of the nanocrystal. Similar behavior has been noted for quenching by CT from the QD to dopamine acting as an electron acceptor or, alternatively, by CT to the QD from the Ru(II) complex.[19,20,27] Second is the consistent quenching of QD samples when paired with Os-pep over a broad range of PL, spanning the spectrum from 520 to 625 nm. This behavior is again quite analogous to the observed quenching of QDs with PL ranging from 510 to 635 nm by the aforementioned Ru complex.[27] Indeed, this broad quenching response, and its similarity to what was observed for interactions with Ru(II), in conjunction with the low overall spectral overlap, led us to initially speculate that CT was responsible for QD quenching. The next item is the lack of a rise time component for the measured Os sensitization, although this may not be significant, as the QD is effectively quenched in <2 ns. Differences between predicted and experimental FRET distances for 530 and 550 nm QD interactions with Os-pep also suggest that the Förster analysis, as applied to these two samples, may not adequately reflect the underlying ET processes. It should be noted that a 15–20% deviation from predicted distance in a FRET complex may also reflect effects from QD size, peptide conformation, linker dynamics, and ligand interactions.

The last item not conforming to classical FRET expectations is that the sensitized Os lifetimes increase far more than would be expected. This is also perhaps the most complex result to interpret, although we do note that similar results have been reported for other QD–Os(II) ET systems (*vide infra*).[63] During FRET, the sensitized acceptor lifetime should increase only when the donor has a significantly longer excited-state

lifetime relative to it and the ET rate does not prohibit it.[61] For example, pairing similar 530 nm QDs (τ_{av} 14.4 ns) with Cy3 dye acceptors increased the latter's sensitized lifetime to 4.70 ns from the native lifetime of 1.33 ns. This ~3.5 times increase reflects both the ET process and the time required by the acceptor to dissipate the longer-lifetime donor energy.[47] Increases in acceptor-sensitized lifetime should not be observed when the acceptor has a longer native lifetime than that of the donor. However, this is indeed observed here when pairing the current 530 nm QDs (τ_{av} 14.1 ns) with the Os-bpy-labeled peptide, where the native lifetime of 30.8 ns increases >1.5 times to a maximum of 53.2 ns at an acceptor valence of 7.5.

We ascribe this somewhat counterintuitive observation to the presence and possible contributions from a number of complex and perhaps even overlapping processes. The first is that of increasing direct Os-bpy excitation as the QD valence increases (see Table 3), which may be concurrent with the issue of homoFRET between Os-bpy molecules heterogeneously arrayed on the QD surface. As the ratio of assembled peptide increases, the probability of peptides being closer to each other on the QD surface also increases significantly. Modeling the QD peptide spacing distribution as valence increases assuming equivalent "perfect" spacing (see Supporting Information) suggests that at a ratio of just 32 peptides the spacing on the QD surface would be very close to the predicted Os-bpy R_0 value of 13.6 A for homoFRET interactions. Again the nominal $R_0 + 0.5R_0$ rule[62] suggests that any two Os-bpy acceptors would have to be within only 20.4 Å or less for homoFRET; this spacing would occur at even lower valence than 32 peptides. In reality, the peptides will not assemble onto the QDs with such perfect spacing. They will occupy available sites on the surface where not precluded by the PEG ligand.[39] We thus surmise that some peptides may be in very close proximity of each other (<13.6 A) at far lower ratios and in a more "patchy" distribution. Os-bpy homoFRET interactions are energetically neutral and not unfavored should the distance requirements be met. Regardless of the actual distribution on the QD surface, the probability for Os-bpy homoFRET increases significantly as valence increases. Additionally, the native Os-bpy photophysical characteristics can be subject to change once self-assembled to the QD surface and surrounded by, or interacting with, the PEGylated ligands. Such changes in solvation and environment are not uncommon to dyes and have also been suggested as the mechanism behind changes in Ru-phenanthroline to QD CT following intestinal fatty acid binding protein structural rearrangement.[25,61] Lastly, the numerous MLCT states may also be able to interact with or contribute in this configuration. Cumulatively, the presence and complex interactions of all these dynamic processes, along with the possibility for "ping-pong" ET in metal CT complexes,[64] make it extremely challenging to elucidate the underlying mechanisms behind the increases in Os-acceptor-sensitized lifetime.

Nevertheless, to look for possible contributions or the underlying signature of a CT component within the kinetic quenching data, we modeled the time dependence of the ET process for the 530 nm QD–Os-bpy complex for both FRET and electron transfer mechanisms. It should be noted that, for simplicity, these models only examine the kinetic features observed and do not incorporate other intrinsic factors such as distance dependency. The following sets of equations were derived to describe the decay dynamics (the full derivation is provided in the Supporting Information). The time dependence of the 530 nm QD decay is given by

$$N_{QD}(t) = \alpha_{QD}\tau_N \exp(-t/\tau_N) \quad (1)$$

where $N_{QD}(t)$ is the time-dependent population of excited state QDs, α_{QD} is the probability of QD excitation with light intensity and frequency $I(\omega)$, $1/\tau_N = 1/\tau_{QD} + N_q/\tau_E$ is the total rate of the QD population decay, τ_{QD} is the decay rate of the QD in the absence of acceptors, N_q is the number of Os-bpy complexes that surround the central QD, and τ_E is the ET rate from a QD to a single Os-bpy complex. It is important to point out that, taken by itself, the QD decay dynamics are not informative enough to differentiate between FRET and CT. The time dependence, $N_{Os}(t)$, for the Os-bpy complex acceptor decay due to FRET is described by

$$N_{Os}(t) = \frac{\alpha_{QD}\tau_N\tau_{Os}}{\tau_E}\left[\frac{\tau_N}{\tau_{Os}-\tau_N}\left(\exp\left(\frac{-t}{\tau_{Os}}\right) + \exp\left(\frac{-t}{\tau_N}\right)\right) + \exp\left(\frac{-t}{\tau_{Os}}\right)\right] + \alpha_{Os}N_q\tau_{Os}\exp\left(-\frac{t}{\tau_{Os}}\right) \quad (2)$$

where α_{Os} is the probability of Os-bpy complex excitation by light with intensity and frequency $I(\omega)$. This equation describes the decay kinetics assuming a FRET mechanism based on measured absorption coefficients and lifetime data and (again) does not attempt to incorporate distance dependences. This equation predicts that, after switching off the excitation source, the PL signal from the Os complex increases slightly on the time scale of τ_N and then decays with the Os complex time constant τ_{Os}. The last term in the equation takes direct excitation of the Os-bpy complexes into account.

In the case of CT the time dependence of $N_{QD}(t)$ is described by a very similar dependence, with τ_N replaced by τ_e, where $1/\tau_e = 1/\tau + N_q/\tau_{CT}$ is the total charge transfer rate and τ_{CT} is the electron transfer time between a single QD and a single Os-bpy complex. The time dependence, $N_{Os}(t)$, for the Os-bpy complex decay due to CT is significantly different than that expected from FRET, in that the Os complex

luminescence is quenched immediately, and the time dependence is described by

$$N_{Os}(t) = \frac{\alpha_{QD}\tau_{CT}\tau_{Os}}{\tau_e}\left[-\frac{\tau_{CT}}{\tau_{Os}-\tau_{CT}}\left(\exp\left(\frac{-t}{\tau_{Os}}\right) - \exp\left(\frac{-t}{\tau_{CT}}\right)\right) - \exp\left(\frac{-t}{\tau_{Os}}\right)\right] + \alpha_{Os}\tau_{Os}\exp\left(\frac{-t}{\tau_{Os}}\right) \quad (3)$$

where $1/\tau_{CT} = 1/\tau + N_q/\tau_e$ is the total charge transfer decay rate of the QD population and τ_e is the electron transfer rate between a single QD and a single Os-bpy complex. In this case, the Os-bpy complex is quenched on a time scale, τ_{ET}, and then decays with the characteristic Os-bpy decay time, τ_{Os}. Figure 6B illustrates the behavior predicted by the model for both the FRET and electron transfer mechanisms for the Os-bpy decay at a nominal valence of 7.5 Os/QD. The normalized Os experimental decay data collected at the same valence are plotted superimposed over the two modeled decay profiles. The FRET-sensitized Os-bpy emission decay should reflect the contribution from the QD donor at early times and then follow the intrinsic Os-bpy decay rate at longer times. CT would manifest a more rapid decay initially, followed by the intrinsic Os-bpy decay with a lower overall magnitude. Clearly, the decay characteristics of the QD-Os-bpy complex are best described by a FRET mechanism. Benson previously suggested a related model based on QD quenching that also took the different distance dependencies of the two ET processes into account.[26] Interestingly, these predicted a similar kinetic appearance for the two types of quenching profiles at a separation distance analogous to those found in our system.

There are several other reports of QD interactions with acceptor molecules displaying both fluorescent and redox-active properties, where both mechanisms have been either postulated or examined in some detail. McLaurin reported on a system that is perhaps the closest to ours.[63] Two Os(II) polypyridyl complexes, with surrounding chelating ligands that differ slightly from ours, $[Os(bpy)_2(Nbpy)](PF_6)_2$ or $[Os(Ph_2phen)_2(Nbpy)](PF_6)_2$ as compared to our $[Os(bpy)_2(phen\text{-}NH_2)](PF_6)_2$, were conjugated to aqueous-QD surface ligands to assemble two-photon QD-sensitized ratiometric oxygen sensors. Consistent with our data, the authors noted increases in their Os complex emission when attached to, and sensitized by, the QD. However, in contrast to our results, they observe Os emission in the QD complex shifting toward shorter wavelengths by 35−49 nm (bluing) and also noted that the sensitized Os emission was enhanced by nearly *10-fold*. The latter effects were ascribed to exclusion of water from the Os complex solvation sphere following conjugation to the *N*-octylamine-modified poly(acrylic acid) they used to surface-functionalize the QDs. These are mechanistically analogous to the effects of changes in solvation and environment we discuss above in relation to the observed Os-bpy sensitization on the QD. Lack of an analogous *10-fold* change in our system leads us to conclude that our QD−Os complexes probably remain partially solvated as expected given our use of discrete PEG ligands. The presence of O_2 could be another potential contributor to this difference, as it was excluded from their experimental format. Although electron transfer in their system could not be unambiguously ruled out, QD−Os interactions were similarly ascribed to FRET.

Lian *et al.* used both FSTA and steady-state fluorescence to examine 550 nm emitting CdSe QD quenching by adsorbed rhodamine B (RhB) within an organic environment.[35,36] They concluded that both processes were present and estimated that only ~16% of the QD excitons decayed by FRET to the RhB despite the remarkably similar 35 Å R_0 value as compared to our system. The remaining 86% of excitons proceeded efficiently through electron transfer to RhB within 120 ps for a 1:1 complex. Depending on the number of adsorbed RhB molecules, electron transfer could occur at nearly 100% within 54 ps for a 1:1.5 complex, yielding a charge-separated state with an average lifetime of ~1 μs at 2.0 nm distance. Similar to our results, they note increased quenching and decreasing QD lifetimes for higher RhB ratios. Using FSTA to quantitate both FRET and ET, they found that at these shorter distances ET was more efficient. In another example, Shen quenched 550 nm emitting CdTe QDs by electrostatically coupling methylene blue dye acceptors to their surfaces and then showed that added DNA could displace the acceptor and increase the QD PL.[34] In this case, the low Förster radius of ~8 Å coupled to the low QD QY of ~3% led the authors to conclude that the observed QD quenching resulted from an electron transfer process.

There have also been studies that more definitively demonstrated the presence of both ET processes within QD conjugates. Burda was able to elucidate the presence of a non-Förster-type behavior in QD−phthalocyanine conjugates.[57,58] By examining a series of increasingly larger QD donors, ET efficiency was found not to follow a linear dependence on the spectral overlap predicted from Förster theory;[57] this is in contrast to the current data set. In particular, the involvement of QD surface states in ET was shown to contribute to their findings. A notable example that demonstrated both ET processes occurring was reported by the Ford group, where they analyzed ET between CdSe/ZnS QDs and salts of *trans*-$[Cr(cyclam)X_2]^+$ joined by electrostatic assembly, where X was Cl, ONO, or CN.[65] When X was Cl or ONO, the complexes exhibited significant acceptor absorption that matched the QD emission, resulting in quenching

of the QD band-edge emission *via* FRET. Conversely, the QD band-edge emission was not efficiently quenched by *trans*-$[Cr(cyclam)(CN)_2]^+$ due to poor spectral overlap. However, all three salts effectively quenched the deep trap luminescence from the QD *via* ultrafast CT. Thus, while two of the complexes were quenching the band-edge luminescence *via* FRET, they were also involved in CT with the QD surface trap states. The absence or presence of strong spectral overlap with a set of QD donors was also noted for a methylviologen acceptor when moving from a 2^+ to a singly reduced state, although this effect was not directly correlated with ET.[66] Similarly, Raymo utilized photochromic acceptor compounds to switch between different QD quenching pathways.[67−69] Here the acceptor moieties could be optically switched and structurally rearranged from a conformation that had significant spectral overlap with QD donor emission (FRET quenching) to one that did not, but was still capable of strong QD quenching (ET quenching).

Despite these elegant demonstrations, it still remains unclear how QD quenching by FRET or CT will compete when the possibility for both pathways exists simultaneously. Several variables are clearly critical to this including whether the system is suspended in organic or aqueous media, if the acceptor is adsorbed to the QD surface or displaced away from it in space at some nominal distance, the nature of the molecular connection between the QD and the acceptor, the relative rates of each transfer process, and, of course, the driving force for electron transfer along with donor−acceptor spectral overlap. At a first approximation, adsorption to the surface can result in QD surface (trap) states that are far more favorable for CT, especially in organic media. In contrast, placing the acceptor away from the QD donor surface in an aqueous environment may make FRET far more favorable.

Here, we confirm previous findings by McLaurin[63] and provide very strong evidence that Os(II) polypyridyl complexes interact with CdSe/ZnS QDs almost exclusively by FRET in aqueous environments regardless of the possibility for a competing CT process. These results, however, directly contrast with the interactions of QDs with structurally similar Ru(II) polypyridyl complexes in aqueous environments.[20,21,25,26] Further, it remains hard to reconcile our results along with many of the examples cited above. Clearly, more factors are involved in dictating which pathway is accessed in a given situation. With the continued interest in coupling QD donors to FRET acceptors for biosensing and photodynamic therapy sensitization[1] or to redox acceptors for CT and separation in light-harvesting applications,[17] where possibilities for both ET pathways will likely be present, far more research is warranted to fundamentally understand these processes and provide a predictive capability and ultimately a mechanism to control which is manifest in a desired configuration.

MATERIALS AND METHODS

Materials. CdSe/ZnS core/shell ($\lambda_{em\ max.}$ = 520, 530, 550 nm) QDs were synthesized from organometallic precursors as previously described.[70] Custom Qdot 625 nm emitting ITK organic QDs were generously provided by Life Technologies (Eugene, OR, USA). The native organic-functionalized QDs were made hydrophilic *via* cap exchange with poly(ethylene glycol)-appended dihydrolipoic acid ligands (DHLA-PEG-OCH_3, PEG average molecular weight ~750) as reported.[71,72] See Supporting Figure S1 for the ligand structure. The osmium(II) polypyridyl complex, $[Os(bpy)_2(phen\text{-}NCS)](PF_6)_2$ (bpy = 2,2′-bipyridine, phen = phenanthroline), was synthesized as described[37] from $(NH_4)_2[OsCl_6]$ (Sigma-Aldrich, St. Louis, MO, USA). The amine-reactive isothiocyanate group was installed by treating $[Os(bpy)_2(phen\text{-}NH_2)](PF_6)_2$ (phen-NH_2 = 5-amino-1,10-phenanthroline) with thiophosgene. We note that this same Os complex was recently utilized to electrochemically monitor DNA hybridization kinetics.[73]

The reactive Os−isothiocyanate complex was used to site-specifically label the unique N-terminal primary amine on the peptide GSGAAAGLS$(His)_6$-$CONH_2$ (MW = 1513, $CONH_2$ is a C-terminal amide blocking the carboxyl group). This peptide was custom synthesized using standard *in situ* neutralization cycles for Boc-solid-phase-peptide synthesis (Boc-SPPS) as described.[74] Peptide labeling and purification procedures are quite similar to those described in ref 75. Briefly, 1 mg of peptide was dissolved in 1 mL of 0.136 M sodium tetraborate buffer pH 8.6 and combined with excess Os−isothiocyanate complex overnight at 4 °C. Unreacted Os complex was removed by loading the reaction onto three consecutive 0.5 mL columns of Ni-nitrilotriacetic acid-agarose. Columns were washed with 10 mL of phosphate-buffered saline (PBS, 137 mM NaCl, 10 mM phosphate, 3 mM KCl, pH 7.4) before the labeled Os-pep was eluted with 300 mM imidazole in PBS. Os-labeled peptide was then desalted and imidazole removed using a reverse-phase oligonucleotide purification cartridge (OPC, ABI Foster City, CA, USA). The cartridge was primed by first washing with 3 mL of acetonitrile followed with 3 mL of 2 M triethylamine acetate (TEAA) buffer before loading Os-labeled peptide. The column was washed with 50 mL of 0.02 M TEAA, and the labeled peptide eluted, using 1 mL of 70% acetonitrile in distilled/deionized H_2O. Desalted Os-pep was quantitated by UV−visible spectroscopy (Os complex absorbance 12 500 M^{-1} cm^{-1} at 490 nm) before being aliquoted, dried down, and stored in a desiccator at −20 °C until required.

Assembling Quantum Dot−Os-Labeled Peptide Conjugates. Osmium-labeled peptide stock solutions were prepared for each experimental format by dissolving the lyophilized peptide in 95:5 deionized H_2O/DMSO and then self-assembled to QDs at the indicated desired ratios in 1× PBS for ~30 min. Dissolution of the peptide stocks was initiated with the DMSO acting as a carrier, and then the H_2O was added to bring up the volume. Approximately 30 pmol of QD was used per assembly in a total volume of 150 μL, corresponding to a final QD concentration of 0.2 μM.

Spectroscopic Analysis. *UV−Vis Absorbance.* Electronic absorption spectra were recorded using an HP 8453 diode array spectrophotometer (Agilent Technologies, Santa Clara, CA, USA).

Steady-State Fluorescent Data. QD PL spectra were collected on a Tecan Safire dual monochromater multifunction microtiter plate reader (Tecan, Research Triangle Park, NC, USA).

Samples were excited at 370 nm, which corresponds to an Os complex absorption minimum. Corresponding emission spectra from the osmium-peptide were collected on a Spex Fluorolog-3 spectrophotometer (Jobin Yvon Inc., Edison, NJ, USA) equipped with a Spectrum One CCD-3000 detector and a 450 nm CVI long wave pass filter (λ_{excite} = 350 nm). In some cases, nonlinear near-IR detector responses for the Os-emission data collected on the Tecan were corrected using a spectral correction file derived from adjusted control data collected on the Spex Fluorolog.

Excited-State Fluorescent Lifetimes. Two different instrumental systems were utilized to collect excited-state lifetime data. The first was a time-correlated single-photon-counting instrumental system.[46,76] Laser excitation consisted of a synchronously pumped and cavity-dumped dye laser (305 nm), pumped by the second harmonic of an Nd:YLF laser (527 nm, 100 MHz). The dye laser contained a single plate birefringent filter tuned to produce laser oscillation at 610 nm and pulse width of ~1 ps fwhm. The dye laser was cavity-dumped at 1 MHz and frequency doubled using a potassium dihydrogen phosphate nonlinear crystal. Sample fluorescence was spectrally filtered with a monochromator (bandpass ~10 nm) and detected with a cooled microchannel plate PMT (Hamamatsu R2809U-11, Shizuoka Japan). Temporal response function of the system was measured to a fwhm of *ca.* 50 ps. Multiexponential QD PL decay traces (lifetimes) were fitted with an average of 3−4 lifetime components as derived from the fractional amplitude of the positive decay components (% of total amplitude) using FluoFit (Picoquant, Berlin Germany).

The second system used to collect data on the Os-pep-sensitized emission consisted of a 375 nm Becker & Hickl diode laser excitation source with a 50 ps pulse width, operating at 20 MHz utilizing an average power of 0.5 mW. Fluorescence was collected and dispersed using a 1/4-m monochromator, and the signals were detected with a Hamamatsu 8309U-50 MCP-PMT. Signals were processed using a Becker & Hickl time-correlated single-photon-counting system. QD emission was monitored at 530 nm, and emission from the osmium complex was monitored at 740 nm. A correction was applied to the data during processing, as some changes in the baseline were noted. The correction procedure assumes that the baseline consists of a constant contribution that is due to detector noise and a component that decays according to the kinetics of the luminescent species. The baseline noise was recorded by blocking the laser excitation and collecting background for the appropriate collection time. This constant background level was subtracted from the raw fluorescence signal. The luminescence tails between 4 and 44 ns were fit to single-exponential decay functions. The fitting constants were used to calculate an extended decay curve out to 100 ns. The calculated decay curves were then used to approximate the full sloping baselines, which were then subtracted from the data. The resulting data were then analyzed using a PicoQuant fitting routine.

Transient Absorption. Optical transient absorption measurements were performed with an apparatus based on a commercial amplified Ti:sapphire laser system (Spectra-Physics Mira oscillator and Spitfire Pro amplifier) at 1.7 kHz and carried out at the Center for Nanoscale Materials, Argonne National Laboratory. A small amount of the amplifier output was used to generate the white light continuum probe, and the remaining 95% went through an optical parametric amplifier to produce 415 nm excitation pulses at 0.7 μJ/pulse. The data were collected through a Helios spectrometer (Ultrafast Systems), where the probe is delayed relative to the pump on a mechanical delay line. The pump beam is chopped at half the repetition rate of the laser, so that the absorption change (ΔA) can be measured as a function of delay time, where $\Delta A = -\log(I_{pump+probe}/I_{probe})$. The data were chirp-corrected using a solvent blank to within 100 fs over the spectral range of 440 to 760 nm used here. The samples were placed in a 2 mm quartz cuvette and stirred during the acquisition. The widths of the pump and probe pulses were estimated at about 120 fs. The transient absorption changes for a particular probe wavelength as a function of time were analyzed by fitting the kinetics with a multiexponential model convoluted with a Gaussian instrument response function with a 300 fs fwhm.

Förster Resonance Energy Transfer Analyses. For each set of experimental data collected, the areas under the PL spectra were integrated using SigmaPlot and corrected for the direct-acceptor excitation component by comparison to samples collected from directly excited acceptor-only control samples. The resulting data were used to determine the FRET efficiency E_n (n = number of acceptors/QD) using[61]

$$E_n = \frac{(F_D - F_{DA})}{F_D} \quad (4)$$

where F_D and F_{DA} are the fluorescence intensities of the donor in the absence and presence of acceptor(s), respectively. Förster theory was used to determine the center-to-center (QD-to-Os) separation distance from the FRET E analysis using

$$r = R_0\left(\frac{n(1-E)}{E}\right)^{1/6} \quad (5)$$

where n is the ratio or discrete number of acceptors arrayed around the QD and R_0 is the Förster distance corresponding to 50% ET for a single donor−acceptor pair and is determined by[43,61]

$$R_0 = 9.78\times10^3[\kappa^2 \check{n}^{-4} Q_D J(\lambda)]^{1/6} \quad (6)$$

where $\check{n}$ is the buffer medium refractive index, Q_D is the quantum yield of the donor, $J(\lambda)$ is the spectral overlap integral function, and κ^2 is the dipole orientation factor. We use a value of 2/3 for the latter, as this is appropriate for the random dipole orientations found within our self-assembled configurations as described.[1,43] Equation 5 assumes a centrosymmetric distribution of FRET acceptors arrayed around the central QD donor.[1,43] A Poisson distribution function was used as described in ref 44 to account for heterogeneity in conjugate valence during self-assembly when high FRET efficiencies were encountered with low ratios.

Wavelength-Dependent FRET Analyses. As QD donor emissions are inherently narrow, their spectral overlap with a given acceptor will vary as a function of changes in the absorption spectrum ε_A, giving rise to a wavelength-dependent FRET rate.[48] The spectral overlap function $J(\lambda)$ in this configuration is directly proportional to

$$J(\lambda) \approx \varepsilon_A(\lambda)\lambda^4 \quad (7)$$

where ε_A is the acceptor absorption spectrum. This assumes a constant distance r between donor and acceptor for all interactions. A wavelength-dependent FRET quenching rate for this process can be obtained for QDs emitting at a specific wavelength λ by monitoring variations in the ensemble emission spectrum $S_n(\lambda)$ in the presence of n acceptors with[48]

$$k_{FRET}(\lambda) \propto \frac{1}{n}\left(\frac{S_0(\lambda)}{S_n(\lambda)} - 1\right) \quad (8)$$

where $S_0(\lambda)$ is the signal from the QDs alone without acceptors.

Conflict of Interest: The authors declare no competing financial interest.

Acknowledgment. The authors acknowledge NRL, the NRL NSI, ONR, and DTRA JSTO MIPR #B112582M. J.B.B.-C. acknowledges a Marie Curie IOF. A.M.S. acknowledges the ANSER Center, an Energy Frontier Research Center funded by the U.S. Department of Energy, Office of Science, Office of Basic Energy Sciences, as well at the Center for Functional Nanomaterials at Argonne National Laboratory for use of their femtosecond transient absorption system.

Supporting Information Available: Additional experimental details and data, ligand structure, differential absorption, ET model derivation, and electrochemistry. This material is available free of charge *via* the Internet at http://pubs.acs.org.

REFERENCES AND NOTES

1. Medintz, I. L.; Mattoussi, H. Quantum Dot-Based Resonance Energy Transfer and its Growing Application in Biology. *Phys. Chem. Chem. Phys.* **2009**, *11*, 17–45.
2. Algar, W. R.; Krull, U. J. New Opportunities in Multiplexed Optical Bioanalyses Using Quantum Dots and Donor-Acceptor Interactions. *Anal. Bioanal. Chem.* **2010**, *398*, 2439–2449.
3. Callan, J. F.; Mulrooney, R. C.; Kamila, S.; McCaughan, B. Anion Sensing with Luminescent Quantum Dots—A Modular Approach Based on the Photoinduced Electron Transfer (PET) Mechanism. *J. Fluoresc.* **2008**, *18*, 527–532.
4. Shibu, E. S.; Sonoda, A.; Tao, Z.; Feng, Q.; Furube, A.; Masuo, S.; Wang, L.; Tamai, T.; Ishikawa, M.; Biju, V. Photofabrication of Fullerene-Shelled Quantum Dots Supramolecular Nanoparticles for Solar Energy Harvesting. *ACS Nano* **2012**, *6*, 1601–1608.
5. Algar, W. R.; Susumu, K.; Delehanty, J. B.; Medintz, I. L. Quantum Dots in Bioanalysis: Crossing the Valley of Death. *Anal. Chem.* **2011**, *83*, 8826–8837.
6. Dennis, A. M.; Sotto, D.; Mei, B. C.; Medintz, I. L.; Mattoussi, H.; Bao, G. Surface Ligand Effects on Metal-Affinity Coordination to Quantum Dots: Implications for Nanoprobe Self-Assembly. *Bioconjugate Chem.* **2010**, *21*, 1160–1170.
7. Yildiz, I.; Tomasulo, M.; Raymo, F. M. A Mechanism to Signal Receptor—Substrate Interactions with Luminescent Quantum Dots. *Proc. Natl. Acad. Sci. U. S. A.* **2006**, *103*, 11457–11460.
8. Halivni, S.; Sitt, A.; Hadar, I.; Banin, U. Effect of Nanoparticle Dimensionality on Fluorescence Resonance Energy Transfer in Nanoparticle—Dye Conjugated Systems. *ACS Nano* **2012**, *6*, 2758–2765.
9. Dennis, A. M.; Bao, G. Quantum Dot-Fluorescent Protein Pairs as Novel Fluorescence Resonance Energy Transfer Probes. *Nano Lett.* **2008**, *8*, 1439–1445.
10. Geissler, D.; Charbonniere, L. J.; Ziessel, R. F.; Butlin, N. G.; Lohmannsroben, H. G.; Hildebrandt, N. Quantum Dot Biosensors for Ultrasensitive Multiplexed Diagnostics. *Angew. Chem., Int. Ed.* **2010**, *49*, 1396–1401.
11. Morgner, F.; Geissler, D.; Stufler, S.; Butlin, N. G.; Lohmannsroben, H. G.; Hildebrandt, N. A Quantum-Dot-Based Molecular Ruler for Multiplexed Optical Analysis. *Angew. Chem., Int. Ed.* **2010**, *49*, 7570–7574.
12. Algar, W. R.; Wegner, D.; Huston, A.; Blanco-Canosa, J.; Stewart, M. H.; Armstrong, A.; Dawson, P. E.; Hildebrandt, N.; Medintz, I. L. Quantum Dots as Simultaneous Acceptors and Donors in Time-Gated Förster Resonance Energy Transfer Relays: Characterization and Biosensing. *J. Am. Chem. Soc.* **2012**, *134*, 1876–1894.
13. Pons, T.; Medintz, I. L.; Sapsford, K. E.; Higashiya, S.; Grimes, A. F.; English, D. S.; Mattoussi, H. On the Quenching of Semiconductor Quantum Dot Photoluminescence by Proximal Gold Nanoparticles. *Nano Lett.* **2007**, *7*, 3157–3164.
14. Shafran, E.; Mangum, B. D.; Gerton, J. M. Energy Transfer from an Individual Quantum Dot to a Carbon Nanotube. *Nano Lett.* **2010**, *10*, 4049–4054.
15. Weaver, J. E.; Dasari, M. R.; Datar, A.; Talapatra, S.; Kohli, P. Investigating Photoinduced Charge Transfer in Carbon Nanotube-Perylene-Quantum Dot Hybrid Nanocomposites. *ACS Nano* **2010**, *4*, 6883–6893.
16. Mountrichas, G.; Sandanayaka, A. S. D.; Economopoulos, S. P.; Pispas, S.; Ito, O.; Hasobe, T.; Tagmatarchis, N. Photoinduced Electron Transfer in Aqueous Carbon Nanotube/Block Copolymer/CdS Hybrids: Application in the Construction of Photoelectrochemical Cells. *J. Mater. Chem.* **2009**, *19*, 8990–8998.
17. Anderson, N. A.; Lian, T. Q. Ultrafast Electron Transfer at the Molecule-Semiconductor Nanoparticle Interface. *Annu. Rev. Phys. Chem.* **2005**, *56*, 491–519.
18. Wang, C. J.; Shim, M.; Guyot-Sionnest, P. Electrochromic Nanocrystal Quantum Dots. *Science.* **2001**, *291*, 2390–2392.
19. Medintz, I. L.; Stewart, M. H.; Trammell, S. A.; Susumu, K.; Delehanty, J. B.; Mei, B. C.; Melinger, J. S.; Blanco-Canosa, J. B.; Dawson, P. E.; Mattoussi, H. Quantum-Dot/Dopamine Bioconjugates Function as Redox Coupled Assemblies for *in Vitro* and Intracellular pH Sensing. *Nat. Mater.* **2010**, *9*, 676–684.
20. Medintz, I. L.; Pons, T.; Trammell, S. A.; Grimes, A. F.; English, D. S.; Blanco-Canosa, J. B.; Dawson, P. E.; Mattoussi, H. Interactions between Redox Complexes and Semiconductor Quantum Dots Coupled *via* a Peptide Bridge. *J. Am. Chem. Soc.* **2008**, *130*, 16745–16756.
21. Sandros, M. G.; Gao, D.; Benson, D. E. A Modular Nanoparticle-Based System for Reagentless Small Molecule Biosensing. *J. Am. Chem. Soc.* **2005**, *127*, 12198–12199.
22. Juris, A.; Balzani, V.; Barigelletti, F.; Campagna, S.; Belser, P.; Vonzelewsky, A. Ru(II) Polypyridine Complexes—Photophysics, Photochemistry, Electrochemistry, and Chemiluminescence. *Coord. Chem. Rev.* **1988**, *84*, 85–277.
23. Marin, V.; Holder, E.; Hoogenboom, R.; Schubert, U. S. Functional Ruthenium(II)- and Iridium(III)-Containing Polymers for Potential Electro-Optical Applications. *Chem. Soc. Rev.* **2007**, *36*, 618–635.
24. Polo, A. S.; Itokazu, M. K.; Iha, N. Y. M. Metal Complex Sensitizers in Dye-Sensitized Solar Cells. *Coord. Chem. Rev.* **2004**, *248*, 1343–1361.
25. Aryal, B. P.; Benson, D. E. Electron Donor Solvent Effects Provide Biosensing with Quantum Dots. *J. Am. Chem. Soc.* **2006**, *128*, 15986–15987.
26. Swain, M. D.; Octain, J.; Benson, D. E. Unimolecular, Soluble Semiconductor Nanoparticle-Based Biosensors for Thrombin Using Charge/Electron Transfer. *Bioconjugate Chem.* **2008**, *19*, 2520–2526.
27. Medintz, I. L.; Farrell, D.; Susumu, K.; Trammell, S. A.; Deschamps, J. R.; Brunel, F. M.; Dawson, P. E.; Mattoussi, H. Multiplex Charge Transfer Interactions between Quantum Dots and Peptide-Bridged Ruthenium complexes. *Anal. Chem.* **2009**, *81*, 4831–4839.
28. Sykora, M.; Petruska, M. A.; Alstrum-Acevedo, J.; Bezel, I.; Meyer, T. J.; Klimov, V. I. Photoinduced Charge Transfer between CdSe Nanocrystal Quantum Dots and Ru-Polypyridine Complexes. *J. Am. Chem. Soc.* **2006**, *128*, 9984–9985.
29. Verma, S.; Kar, P.; Das, A.; Palit, D. K.; Ghosh, H. N. The Effect of Heavy Atoms on Photoinduced Electron Injection from Nonthermalized and Thermalized Donor States of M-II-Polypyridyl (M=Ru/Os) Complexes to Nanoparticulate TiO_2 Surfaces: An Ultrafast Time-Resolved Absorption Study. *Chem.—Eur. J.* **2010**, *16*, 611–619.
30. Verma, S.; Kar, P.; Das, A.; Palit, D. K.; Ghosh, H. N. Interfacial Electron-Transfer Dynamics on TiO_2 and ZrO_2 Nanoparticle Surface Sensitized by New Catechol Derivatives of Os(II)-Polypyridyl Complexes: Monitoring by Charge-Transfer Emission. *J. Phys. Chem. C* **2008**, *112*, 2918–2926.
31. Kuciauskas, D.; Monat, J. E.; Villahermosa, R.; Gray, H. B.; Lewis, N. S.; McCusker, J. K. Transient Absorption Spectroscopy of Ruthenium and Osmium Polypyridyl Complexes Adsorbed onto Nanocrystalline TiO_2 Photoelectrodes. *J. Phys. Chem. B* **2002**, *106*, 9347–9358.
32. Kuciauskas, D.; Freund, M. S.; Gray, H. B.; Winkler, J. R.; Lewis, N. S. Electron transfer Dynamics in Nanocrystalline Titanium Dioxide Solar Cells Sensitized with Ruthenium or Osmium Polypyridyl Complexes. *J. Phys. Chem. B* **2001**, *105*, 392–403.
33. Kumaresan, D.; Shankar, K.; Vaidya, S.; Schmehl, R. H. Photochemistry and Photophysics of Coordination Compounds: Osmium. *Photochem. Photophys. Coord. Compd. II* **2007**, *281*, 101–142.
34. Shen, J. S.; Yu, T.; Xie, J. W.; Jiang, Y. B. Photoluminescence of CdTe Nanocrystals Modulated by Methylene Blue and DNA. A Label-Free Luminescent Signaling Nanohybrid Platform. *Phys. Chem. Chem. Phys.* **2009**, *11*, 5062–5069.
35. Boulesbaa, A.; Huang, Z. Q.; Wu, D.; Lian, T. Q. Competition between Energy and Electron Transfer from CdSe QDs to Adsorbed Rhodamine B. *J. Phys. Chem. C* **2010**, *114*, 962–969.
36. Boulesbaa, A.; Issac, A.; Stockwell, D.; Huang, Z.; Huang, J.; Guo, J.; Lian, T. Ultrafast Charge Separation at CdS

Quantum Dot/Rhodamine B Molecule Interface. *J. Am. Chem. Soc.* **2007**, *129*, 15132–15133.
37. Prasuhn, D. E. Development of Icosahedral Virus Particles as Multivalent Display Scaffolds for Metal Complexes. Ph. D. Thesis, The Scripps Research Institute, La Jolla, CA, 2007.
38. Hermanson, G. T. *Bioconjugate Techniques*, 2nd ed.; Academic Press: San Diego, CA, 2008.
39. Sapsford, K. E.; Pons, T.; Medintz, I. L.; Higashiya, S.; Brunel, F. M.; Dawson, P. E.; Mattoussi, H. Kinetics of Metal-Affinity Driven Self-Assembly between Proteins or Peptides and CdSe-ZnS Quantum Dots. *J. Phys. Chem. C* **2007**, *111*, 11528–11538.
40. Prasuhn, D. E.; Deschamps, J. R.; Susumu, K.; Stewart, M. A.; Boeneman, K.; Blanco-Canosa, J. B.; Dawson, P. E.; Medintz, I. L. Polyvalent Display and Packing of Peptides and Proteins on Semiconductor Quantum Dots: Predicted *versus* Experimental Results. *Small* **2009**, *6*, 555–564.
41. Meyer, T. J. Photochemistry of Metal Coordination-Complexes—Metal to Ligand Charge-Transfer Excited-States. *Pure Appl. Chem.* **1986**, *58*, 1193–1206.
42. Pankuch, B. J.; Lacky, D. E.; Crosby, G. A. Charge-Transfer Excited-States of Osmium(II) Complexes. 1. Assignment of the Visible Absorption-Bands. *J. Phys. Chem.* **1980**, *84*, 2061–2067.
43. Clapp, A. R.; Medintz, I. L.; Mauro, J. M.; Fisher, B. R.; Bawendi, M. G.; Mattoussi, H. Fluorescence Resonance Energy Transfer Between Quantum Dot Donors and Dye-Labeled Protein Acceptors. *J. Am. Chem. Soc.* **2004**, *126*, 301–310.
44. Pons, T.; Medintz, I. L.; Wang, X.; English, D. S.; Mattoussi, H. Solution-Phase Single Quantum Dot Fluorescence Resonant Energy Transfer Sensing. *J. Am. Chem. Soc.* **2006**, *128*, 15324–15331.
45. Dabbousi, B. O.; Rodriguez-Viejo, J.; Mikulec, F. V.; Heine, J. R.; Mattoussi, H.; Ober, R.; Jensen, K. F.; Bawendi, M. G. (CdSe)ZnS Core-Shell Quantum Dots: Synthesis and Optical and Structural Characterization of a Size Series of Highly Luminescent Materials. *J. Phys. Chem. B* **1997**, *101*, 9463–9475.
46. Medintz, I. L.; Pons, T.; Susumu, K.; Boeneman, K.; Dennis, A.; Farrell, D.; Deschamps, J. R.; Melinger, J. S.; Bao, G.; Mattoussi, H. Resonance Energy Transfer between Luminescent Quantum Dots and Diverse Fluorescent Protein Acceptors. *J. Phys. Chem. C* **2009**, *131*, 18552–18561.
47. Boeneman, K.; Prasuhn, D. E.; Blanco-Canosa, J. B.; Dawson, P. E.; Melinger, J. S.; Ancona, M.; Stewart, M. H.; Susumu, K.; Huston, A.; Medintz, I. L. Self-Assembled Quantum Dot-Sensitized Multivalent DNA Photonic Wires. *J. Am. Chem. Soc.* **2010**, *132*, 18177–18190.
48. Pons, T.; Medintz, I. L.; Sykora, M.; Mattoussi, H. Spectrally Resolved Energy Transfer Using Quantum Dot Donors: Ensemble and Single-Molecule Photoluminescence Studies. *Phys. Rev. B* **2006**, *73*, 745302.
49. Burda, C.; Green, T. C.; Link, S.; El-Sayed, M. A. Electron Shuttling across the Interface of CdSe Nanoparticles Monitored by Femtosecond Laser Spectroscopy. *J. Phys. Chem. B* **1999**, *103*, 1783–1788.
50. Burda, C.; Link, S.; Mohamed, M.; El-Sayed, M. A. The Relaxation Pathways of CdSe Nanoparticles Monitored with Femtosecond Time-Resolution from the Visible to the IR: Assignment of the Transient Features by Carrier Quenching. *J. Phys. Chem. B* **2001**, *105*, 12286–12292.
51. Nirmal, M.; Murray, C. B.; Bawendi, M. G. Fluorescence-Line Narrowing in CdSe Quantum Dots—Surface Localization of the Photogenerated Exciton. *Phys. Rev. B* **1994**, *50*, 2293–2300.
52. Nirmal, M.; Norris, D. J.; Kuno, M.; Bawendi, M. G.; Efros, A. L.; Rosen, M. Observation of the "Dark Exciton" in CdSe Quantum Dots. *Phys. Rev. Lett.* **1995**, *75*, 3728–3731.
53. Kucur, E.; Riegler, J.; Urban, G. A.; Nann, T. Determination of Quantum Confinement in CdSe Nanocrystals by Cyclic Voltammetry. *J. Chem. Phys.* **2003**, *119*, 2333–2337.
54. Amelia, M.; Avellini, T.; Monaco, S.; Impellizzeri, S.; Yildiz, I.; Raymo, F. M.; Credi, A. Redox Properties of CdSe and CdSe-ZnS Quantum Dots in Solution. *Pure Appl. Chem.* **2011**, *83*, 1–8.
55. Impellizzeri, S.; Monaco, S.; Yildiz, I.; Amelia, M.; Credi, A.; Raymo, F. M. Structural Implications on the Electrochemical and Spectroscopic Signature of CdSe-ZnS Core-Shell Quantum Dots. *J. Phys. Chem. C* **2010**, *114*, 7007–7013.
56. Crespilho, F. N.; Zucolotto, V.; Oliveira, O. N., Jr.; Nart, F. C. Electrochemistry of Layer-by-Layer Films. *Int. J. Electrochem. Sci.* **2006**, *1*, 194–214.
57. Dayal, S.; Lou, Y.; Anna, C. S.; Berlin, J. C.; Kenney, M. E.; Burda, C. Observation of Non-Förster-Type Energy-Transfer Behavior in Quantum Dot-Pthalocyanine Conjugates. *J. Am. Chem. Soc.* **2006**, *128*, 13974–13975.
58. Dayal, S.; Burda, C. Surface Effects on Quantum Dot-Based Energy Transfer. *J. Am. Chem. Soc.* **2007**, *129*, 7977–7981.
59. Chen, J. L.; Zheng, A. F.; Gao, Y. C.; He, C. Y.; Wu, G. H.; Chen, Y. C.; Kai, X. M.; Zhu, C. Q. Functionalized CdS Quantum Dots-Based Luminescence Probe for Detection of Heavy and Transition Metal Ions in Aqueous Solution. *Spectrochim. Acta Part A* **2008**, *69*, 1044–1052.
60. Trammell, S. A.; Yang, S. A.; Sykora, M.; Fleming, C. N.; Odobel, F.; Meyer, T. J. Molecular Energy Transfer across Oxide Surfaces. *J. Phys. Chem. B* **2001**, *105*, 8895–8904.
61. Lakowicz, J. R. *Principles of Fluorescence Spectroscopy*, 3rd ed.; Springer: New York, 2006.
62. Sapsford, K. E.; Berti, L.; Medintz, I. L. Materials for Fluorescence Resonance Energy Transfer: Beyond Traditional 'Dye to Dye' Combinations. *Angew. Chem., Int. Ed.* **2006**, *45*, 4562–4588.
63. McLaurin, E. J.; Greytak, A. B.; Bawendi, M. G.; Nocera, D. G. Two-Photon Absorbing Nanocrystal Sensors for Ratiometric Detection of Oxygen. *J. Am. Chem. Soc.* **2009**, *131*, 12994–13001.
64. Yarnell, J. E.; Deaton, J. C.; McCusker, C. E.; Castellano, F. N. Bidirectional "Ping-Pong" Energy Transfer and 3000-Fold Lifetime Enhancement in a Re(I) Charge Transfer Complex. *Inorg. Chem.* **2011**, *50*, 7820–7830.
65. Neuman, D.; Ostrowski, A. D.; Mikhailovsky, A. A.; Absalonson, R. O.; Strouse, G. F.; Ford, P. C. Quantum Dot Fluorescence Quenching Pathways with Cr(III) Complexes. Photosensitized NO Production from *trans*-Cr(cyclam)-$(ONO)_2^+$. *J. Am. Chem. Soc.* **2008**, *130*, 168–175.
66. Scholz, F.; Dworak, L.; Matylitsky, V. V.; Wachtveitl, J. Ultrafast Electron Transfer from Photoexcited CdSe Quantum Dots to Methylviologen. *ChemPhysChem* **2011**, *12*, 2255–2259.
67. Raymo, F. M.; Tomasulo, M. Electron and Energy Transfer Modulation with Photochromic Switches. *Chem. Soc. Rev.* **2005**, *34*, 327–336.
68. Raymo, F. M.; Yildiz, I. Luminescent Chemosensors Based on Semiconductor Quantum Dots. *Phys. Chem. Chem. Phys.* **2007**, *9*, 2036–2043.
69. Yildiz, I.; Deniz, E.; Raymo, F. M. Fluorescence Modulation with Photochromic Switches in Nanostructured Constructs. *Chem. Soc. Rev.* **2009**, *38*, 1859–1867.
70. Peng, Z. A.; Peng, X. Formation of High-Quality CdTe, CdSe, and CdS Nanocrystals Using CdO as Precursor. *J. Am. Chem. Soc.* **2001**, *123*, 183–184.
71. Mei, B. C.; Susumu, K.; Medintz, I. L.; Delehanty, J. B.; Mountziaris, T. J.; Mattoussi, H. Modular Poly(Ethylene Glycol) Ligands for Biocompatible Semiconductor and Gold Nanocrystals with Extended pH and Ionic Stability. *J. Mater. Chem.* **2008**, *18*, 4949–4958.
72. Susumu, K.; Oh, E.; Delehanty, J. B.; Blanco-Canosa, J. B.; Johnson, B. J.; Jain, V.; Hervey, W. J.; Algar, W. R.; Boeneman, K.; Dawson, P. E.; *et al.* Multifunctional Compact Zwitterionic Ligands for Preparing Robust Biocompatible Semiconductor Quantum Dots and Gold Nanoparticles. *J. Am. Chem. Soc.* **2011**, *133*, 9480–9496.
73. Buckhout-White, S.; Ancona, M.; Oh, E.; Deschamps, J. R.; Stewart, M. H.; Blanco-Canosa, J. B.; Dawson, P. E.; Goldman, E. R.; Medintz, I. L. Multimodal Characterization of a Linear DNA-Based Nanostructure. *ACS Nano* **2012**, *6*, 1026–1043.
74. Schnolzer, M.; Alewood, P.; Jones, A.; Alewood, D.; Kent, S. B. *In Situ* Neutralization in Boc-Chemistry Solid Phase

Peptide Synthesis. Rapid, High Yield Assembly of Difficult Sequences. *Int. J. Pept. Protein Res.* **1992**, *40*, 180–93.
75. Sapsford, K. E.; Farrell, D.; Sun, S.; Rasooly, A.; Mattoussi, H.; Medintz, I. L. Monitoring of Enzymatic Proteolysis on a Electroluminescent-CCD Microchip Platform using Quantum Dot-Peptide Substrates. *Sens. Actuators, B* **2009**, *139*, 13–21.
76. Clapp, A. R.; Pons, T.; Medintz, I. L.; Delehanty, J. B.; Melinger, J. S.; Tiefenbrunn, T.; Dawson, P. E.; Fisher, B. R.; O'Rourke, B.; Mattoussi, H. Two-Photon Excitation of Quantum Dot-Based Fluorescence Resonance Energy Transfer and its Applications. *Adv. Mater.* **2007**, *19*, 1921–1926.